

Optical properties of discontinuous gold films

S. Norrman, T. Andersson, and C. G. Granqvist

Physics Department, Chalmers University of Technology, Fack, S-402 20 Gothenburg, Sweden

O. Hunderi

Department of Physical Metallurgy, Norwegian Institute of Technology, 7034 Trondheim-NTH, Norway

(Received 31 May 1977)

We prepared discontinuous gold films by ultrahigh-vacuum deposition onto Corning 7059 glass substrates. Optical transmittance at normal incidence was recorded; an anomalous absorption band occurred in the visible range. We described the optical properties within the Maxwell Garnett formalism with proper account taken of a size-dependent dielectric permeability of the islands. These were represented by prolate spheroids with symmetry axis along the substrate; their morphology was characterized by mean eccentricity, log normal distributions of half axes, and average interisland separation. Interactions among the islands were accounted for by following a procedure by Bedaux and Vlieger. The computed transmittances were lowered significantly by even narrow distributions of interparticle separations. This complex situation was simulated by one parameter (the *only* free parameter in our theory); reasonable values yielded computed transmittances in excellent agreement with measurements as long as the islands were not too irregular. Effects of substrate interaction and dielectric pellicles on the islands were shown to be less influential. Hence, the optical properties of discontinuous metal films seem to be governed entirely by the morphology of the islands, and possible effects of modified band structure and/or size quantizations are not manifest.

I. INTRODUCTION

This paper describes a thorough investigation of the optical properties of discontinuous gold films. The wavelength interval of 0.3–2 μm is studied for films with average thicknesses of 1–4 nm, which corresponds to growth from extremely small islands up to a stage in the vicinity of large-scale coalescence. A structure analysis of similarly prepared films was given in Ref. 1.

As an introduction we show by the solid curve in Fig. 1 the optical transmittance for a metal film comprised of tiny islands. The detailed analysis of this type of curve will be the main topic of this paper. The wavelength-dependent transmittance is seen to resemble qualitatively the behavior of individually isolated gold particles prepared by gas evaporation, as given by the dashed curve which is reproduced from a recent work² of two of the present authors. The most salient features of the two curves are the transmittance minimum in the visible range and the high transparency in the infrared. A principally very different behavior is encountered for a well-annealed continuous gold film (dotted curve) which represents bulk properties. For the latter curve it is seen that by going to smaller wavelengths the transmittance is first enhanced, as expected from the free-electron (Drude) theory, but at $\lambda < 0.51 \mu\text{m}$ a sharp decrease occurs due to the onset of interband transitions.

From Fig. 1 it is immediately clear that the discontinuous films exhibit optical properties

which are strikingly different from the bulk behavior. This fact has been known, qualitatively, for a long time, and as early as in 1857 it was proposed by Faraday³ that the brilliant colours observed by him in extremely thin silver and gold films should be ascribed to their aggregated nature. About a century later this supposition was

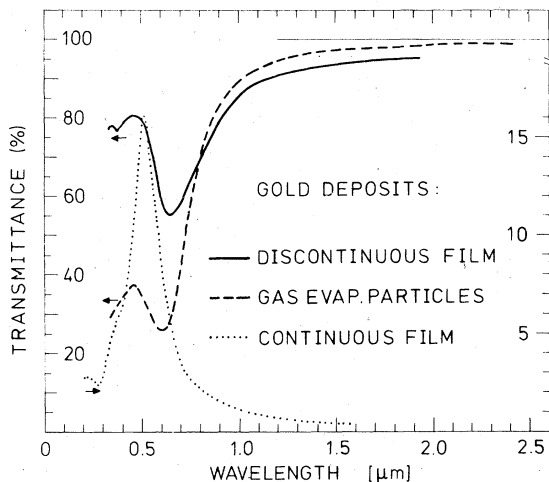


FIG. 1. Comparison of measured transmittance vs wavelength for perpendicular incidence onto gold deposits produced in different ways. Data are shown for a discontinuous film (average thickness 3.0 nm), spherical particles prepared by gas evaporation (the curve is reproduced from Ref. 2) and for a continuous film (thickness 48 nm). Note the different vertical scales for the curves, as indicated by the arrows.

proved by electron microscopy. Particularly during the last 25 years there has appeared a vast number of investigations of the optical properties of discontinuous Cu, Ag, and Au films¹⁻⁴²; a wealth of experimental results has been collected and many theoretical models—all based on the granular film structure—have been used to interpret the data. A motivation for our scrutinizing this well-studied subject anew is therefore in order.

The first reason for this investigation is our previous work¹ on the size distributions and morphology of islands in discontinuous gold films prepared by evaporation in ultrahigh vacuum onto a glass substrate. One of the results was that a good approximation for the three-dimensional island shapes is given by prolate spheroids with their symmetry axes parallel with the substrate plane. As a consequence of the spheroidal forms the internal electric fields in the islands are constant when these are placed in a uniform external field, which makes a detailed theoretical description of the optical properties possible. This leads to the second motivation, which is our recent detailed investigation² of the optical transmittance through deposits of spherical and individually isolated gold particles prepared by evaporation in air. One curve from this work is reproduced in Fig. 1. An elaborate theoretical description, including the roles of dipole-dipole interactions, oxide coatings, etc., was carried out. Here we benefit from this earlier study,² although it should be stressed that the treatment of the optical properties of discontinuous metal films is not identical with that for gas evaporated deposits. The main differences are the nonspherical shapes of islands, the two-dimensional nature of the films, and the possibility of having interactions between substrate and islands. Despite these difficulties we are able to show here that the optical properties of discontinuous metal films can be understood in great detail provided proper account is taken of—in particular—the sizes and shapes of the islands and their dipole-dipole interaction.

The layout of this article is as follows: In Sec. II we report on the experimental results. We describe briefly the details regarding evaporation and electron microscopy of the discontinuous gold films and show then measured optical transmittance through films with different mass thicknesses. Section III gives a careful discussion of the sample characterization, which is obviously a point of extreme importance for a reliable theoretical description of the optical properties. We treat size distributions of the three-dimensional islands and derivations of accurate measures for

average interisland distance and for mean deviation from spherical shape. In Sec. IV we formulate a Maxwell Garnett-type effective-medium theory for a planar array of ellipsoidal islands. Interactions among these are incorporated by defining the "optical" film thickness appropriately, as shown by Bedaux and Vlieger.⁴³ Section V contains a preliminary comparison of computed data and experimental results. The roles of island size and shape—described by a mean eccentricity—are treated. The main conclusion is that calculated transmittances are much too high to be reconciled with the experimental facts. The origin of this discrepancy is dwelt upon in the discussion in Sec. VI. We first regard substrate interaction. This leads to an enhanced absorption, but the effect is estimated to be too small to account for the measured results alone. We then return to the local-field effects and argue, from a modest extension of the work by Bedaux and Vlieger,⁴³ that these can be significantly enhanced by even a narrow distribution of particle-particle separations, which would lead to a lowered transmittance. Our approach introduces one adjustable parameter. Reasonable values of this single parameter yield calculated transmittances being in excellent accord with measured data for the thinner films, whereas the predicted transmittance minima are too narrow for the thicker films, which is expected when considering their very irregular island shapes. In Sec. VII we conclude this paper by a summary of the main results and some final remarks.

Our present study forms part of a larger investigation of gold films which considers also the morphology and size distributions of the islands, the *in situ* conduction of a growing film, the change of conduction following interruption of deposition and the subsequent properties of structurally stable films. These aspects were covered in Refs. 1 and 44-48. Some preliminary results from our optical studies were given in Refs. 49 and 50.

II. EXPERIMENTAL TECHNIQUE AND RESULTS

A. Evaporations

The procedure to prepare the discontinuous films was discussed in Refs. 45 and 48. Below we content ourselves with an outline of the main points of the experimental technique.

Gold of 99.99% purity was deposited onto Corning 7059 glass substrates under ultrahigh vacuum conditions (pressure during evaporation $<4 \times 10^{-9}$ Torr; background pressure $<1 \times 10^{-9}$ Torr). The film size was 5×5 mm. A resistively heated alumina crucible served as vapour source. The substrate temperature was kept constant at 290 ± 5 K, and an

electric field of 20 V/cm was maintained in the substrate plane. The amount of material impinging towards the substrate was recorded on a quartz crystal oscillator microbalance whose reading was converted to an effective thickness for an ideal continuous film having bulk density. The thickness monitor was calibrated to an accuracy of $\pm 5\%$ by use of a Tolansky interference microscope. After the depositions the films were aged in ultrahigh vacuum for more than 20 h. The films (on their backings) were then transferred to a spectrophotometer for measurements of the wavelength dependent optical transmittance. Subsequently a stabilizing amorphous carbon layer was deposited on top of the gold in a conventional bell jar evaporator. The glass substrates were dissolved in 5-vol% HF acid and the free films were then ready for electron microscopy.

Detailed studies were carried out on eight films with mass thicknesses in the range 1.1–4.0 nm; the actual values are listed in the first column of Table I. The films were prepared by evaporation with rates in the interval 0.02–0.04-nm/sec.

B. Electron microscopy

The discontinuous gold films were investigated with a Philips EM 300 electron microscope operated at 100 kV. Its resolution was about 1 nm. Representative pictures for four mass thicknesses t are shown in Fig. 2. It is clear that when t is increased the average size of the islands as well as their irregularity is enhanced. Grain boundaries are visible particularly in some of the larger islands. The elongation is continuing also in the interval $4.0 < t < 5.3$ nm, but once an average thickness of 5.3 nm is exceeded a large scale coalescence occurs and a metalliclike electrical conductivity can be measured along the deposit.

The films were evaporated with an electric field applied in the substrate plane. This may influence the island structure due to field-induced coales-

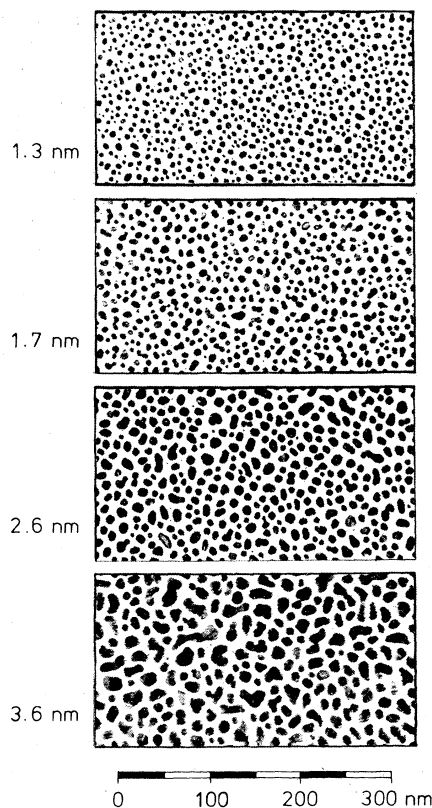


FIG. 2. High-resolution electron micrographs of discontinuous gold films at four different values of the mean film thicknesses. The figures represent regions in the middle of the deposits.

cence of neighboring islands.⁵¹⁻⁶⁰ It is interesting to compare our findings with recent work of Kazmerski and Racine,⁶⁰ who investigated discontinuous gold films prepared by electron beam deposition in ultrahigh vacuum onto Corning 7059 glass under zero applied field conditions. They found that large scale coalescence set in first at $t > 12$ nm, which clearly points at the importance of the

TABLE I. Data for the discontinuous gold films having mass thicknesses t , log-normal distributions of major axes, minor axes, and equivalent projected diameter defined by \bar{a} , \bar{b} , \bar{x} , (median values) and σ_a , σ_b , σ (geometric standard derivations). The mean eccentricity is \bar{e} and the average interisland distance is D .

t (nm)	\bar{a} (nm)	σ_a	\bar{b} (nm)	σ_b	\bar{x} (nm)	σ	\bar{e}	D (nm)
1.1 ± 0.2	5.7	(1.5)	4.5	(1.43)	...	7.3
1.3 ± 0.2	6	(1.35)	5.2	(1.3)	...	8.3
1.5 ± 0.3	8	1.44	5.8	1.22	6.7	1.34	0.79	9.9
1.7 ± 0.3	8.8	1.38	6.8	1.22	7.5	1.3	0.74	10.8
2.6 ± 0.2	11.8	1.36	8.5	1.2	9.8	1.3	0.78	13.6
3.0 ± 0.3	16	1.5	9.8	1.28	13	1.34	0.86	15.8
3.6 ± 0.3	19	1.5	11.5	1.22	15	1.33	0.86	18.1
4.0 ± 0.3	25	(1.6)	13	(1.36)	18.5	(1.4)	0.91	21.5

details of the preparation method for the film. Another striking difference between our discontinuous films and those of some other workers is the absence of large quantities of extremely minute islands; this is amply demonstrated by a comparison between Fig. 2 of Ref. 60 and our Fig. 2, as well as by the results of Ref. 61. The absence of such abnormally small islands in our work facilitates the theoretical description of the optical properties of the films.

From Fig. 2 it is evident that the number density n of islands decreases for increasing average film thickness. This effect is elaborated on in Fig. 3, where we show that the number of islands per cm^2 drops with t approximately as $n \propto e^{-t/t_0}$ (where t_0 is a constant) over the whole thickness range studied. Fig. 3 also shows some data from Hamilton and Logel⁶² who investigated gold deposited onto SiO_2 backings. Their measurements of n vs t fall on a peaked curve, where the increase at $t \lesssim 1$ nm can be ascribed to an enhanced occupancy of nucleation centers, and the subsequent decrease for $t \gtrsim 1$ nm points at the dominance of coalescence processes. It is obvious that if our measurements were extended to smaller thicknesses we would also observe a peaked n vs t variation, and consequently even our thinnest films belong to the coalescence stage of film growth.

The area fraction A of the substrate covered with metal increases with increasing film thickness, as can be seen from Fig. 2. We evaluated A by placing a fine mesh grid over photographs of the discontinuous films and counted the number of nodes which fell on the islands in an area con-

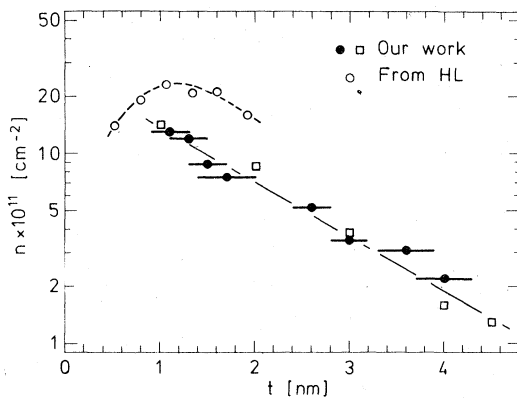


FIG. 3. Number of islands per cm^{-2} vs average film thickness for discontinuous gold films. Filled circles, with estimated errors in the thickness determination shown as horizontal bars, represent the eight samples under present investigation. Squares denote our previous measurements reported on in Ref. 1. Open circles signify results by Hamilton and Logel (Ref. 62). The straight line indicates $n \propto \exp(-t/t_0)$.

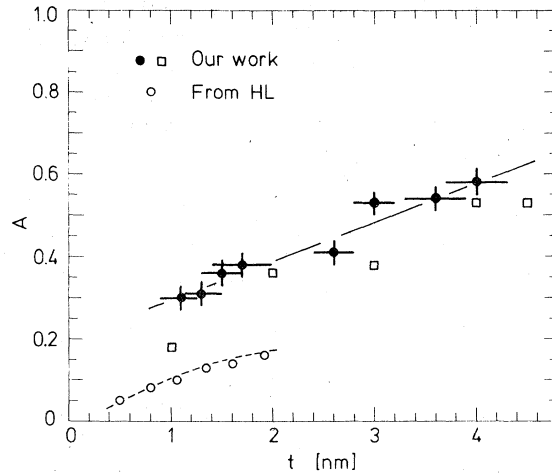


FIG. 4. Area fraction of the substrates covered with metal vs average film thickness for discontinuous gold films. Filled circles with estimated errors shown as bars represent the eight samples under present investigation. Squares denote our previous measurements reported on in Ref. 1. Open circles signify results by Hamilton and Logel (Ref. 62). The straight solid line indicates a linear relation between A and t .

taining more than 1000 islands. As shown in Fig. 4, A increases approximately linearly with t . In the figure we also plot some data from Hamilton and Logel.⁶² For a given thickness their area fractions are much smaller than ours, which once more points at the significance of the detailed conditions at the substrate surface for determining the film structure.

C. Transmittance measurements

Optical transmittance for the discontinuous films on their backings was recorded in the wavelength interval $0.33 < \lambda < 2.5 \mu\text{m}$ with a UNICAM SP 700 double-beam spectrophotometer. The lower wavelength limit was dictated by the transparency of the glass. We always put a substrate with a discontinuous film in one of the light beams and a clean substrate in the other and monitored the ratio between the two transmitted intensities; in this way we diminished significantly the influence from the glass on the recorded data. Only measurements at normal incidence were performed.

Figure 5 shows wavelength dependent transmittance for the eight discontinuous films of Table I. The most noteworthy feature is the transmittance minimum at $0.56 < \lambda_{\text{min}} < 0.70$, i.e., in the visible range. The overall curve shapes are seen to be quite similar for the thinnest films, whereas the thickest ones exhibit wider minima and a slower rise of the transmittance in the infrared.

The thickness dependence of λ_{min} is shown in

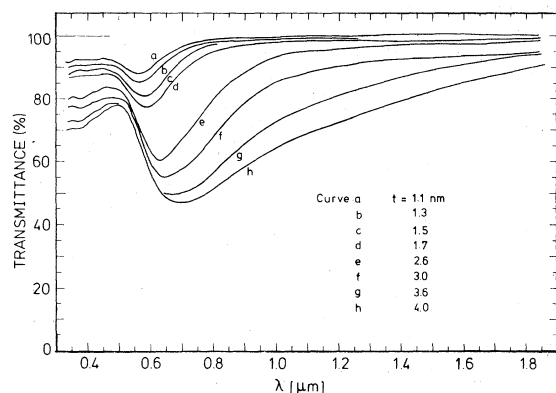


FIG. 5. Transmittance versus wavelength for discontinuous gold films of different thicknesses.

more detail in Fig. 6, where it is seen that the relation is approximately linear over the thickness interval investigated. At zero thickness the intercept with the ordinate occurs at $\lambda_{\min} = 0.51 \mu\text{m}$. Figure 6 also contains some data which were extracted from the literature; the results by Rasigni and Rouard^{21,22} are in good accord with ours, whereas those by Yamaguchi⁸ exhibit a weaker thickness dependence of the transmittance minimum. The discrepancies are probably caused by slightly different conditions for island growth in the various experiments. For completeness it should be mentioned that optical transmittance through discontinuous gold films has been measured also by Doremus,²⁸ Truong and Scott,⁶ and Jarrett and Ward³³; their data are not included in Fig. 6 because either very few results are available for $t \lesssim 4 \text{ nm}$ or the λ_{\min} 's are difficult to determine accurately from the published curves.

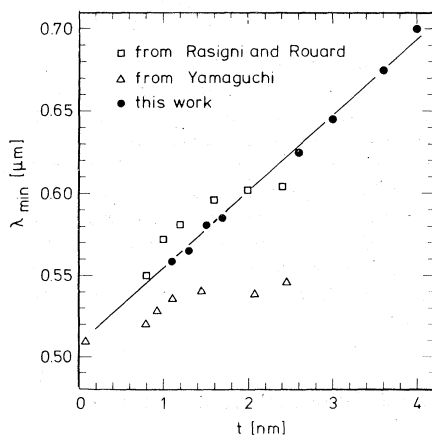


FIG. 6. Wavelength of the transmittance minimum vs thickness for the films in Fig. 5. Data are shown also from articles by Yamaguchi (Ref. 8) and by Rasigni and Rouard (Ref. 22). The straight line represents the relation $\lambda_{\min} = 510 + 46t$ with λ_{\min} and t in nanometers.

Silver films have been even more thoroughly investigated than gold films and numerous results of thickness dependent transmittance minima have been recorded^{4, 8, 13, 21, 22, 27, 35, 38}. As a rule λ_{\min} is roughly proportional to t also for these data.

III. SAMPLE CHARACTERIZATION

The main theme of this article is a detailed theoretical explanation of the optical transmittance data presented in Sec. IIC. To be able to carry out this programme it is obvious that a very accurate description of the film morphology is imperative; such analysis is the topic of this section.

A. Size distributions

It is clear from the electron micrographs in Fig. 2 that the gold islands exhibit a size distribution. Its shape depends on the coarsening mechanism, which is coalescence dominated as was argued for in Sec. IIB. For coalescence growth we can make use of a statistical model^{63, 64} predicting that the logarithm of the island volumes should have a Gaussian distribution. In the case of spherical particles the fractional number of particles Δn per logarithmic diameter interval $\Delta(\ln x_s)$, can then be written

$$\Delta n = f_{\text{LN}}(x_s) \Delta(\ln x_s), \quad (1)$$

with

$$f_{\text{LN}}(x_s) = \frac{1}{(2\pi)^{1/2} \ln \sigma_s} \exp \left[-\frac{1}{2} \left(\frac{\ln(x_s/\bar{x}_s)}{\ln \sigma_s} \right)^2 \right], \quad (2)$$

which defines a *log-normal distribution function*⁶⁵ (LNDF). In Eq. (2), \bar{x}_s denotes the statistical median of the sphere diameters and σ_s is their (geometric) standard deviation. Empirically, the LNDF has been shown to constitute an excellent approximation for experimental size distributions of islands in discontinuous noble metal films,^{1, 63, 64} inert gas evaporated particles,^{2, 64, 66} supported metal catalysts,^{64, 67} and some colloidal particles.⁶⁸

The electron micrographs show that the metal islands look far from circular in particular for the larger thicknesses. A reasonable approximation for the projected area of a film particle is to describe it as being instead an *ellipse* with an area $(\pi/4)ab$, where a is the major axis and b is the minor axis. For practical purposes we let a represent the maximum length of an island while b denotes its largest perpendicular width. Evaluations of a and b for two discontinuous films with different thicknesses are shown in Fig. 7, where the data are also compared with LNDF's. We obtained the correct normaliza-

tion⁶⁹ of the graphs by plotting a versus $(\Delta a/a)Nf_{LN}(a)$ (and correspondingly for b), where Δa is the constant interval in the size histogram and N is the total number of particles in the evaluation. It is seen that the asymmetric, bell shaped LNDF's are good approximations in particular at $t=3$ nm, whereas the agreement at $t=1.5$ nm is more dubious. Such fits define median lengths for the axes, \bar{a} and \bar{b} , as well as their standard deviations, σ_a and σ_b ; the actual values of these quantities are given in Table I for all samples.

We simplify the treatment of the particle shapes by defining also an "equivalent projected diameter" as

$$x = (ab)^{1/2}. \quad (3)$$

From Fig. 7 it is found that also x exhibits an LNDF, which is defined by \bar{x} and σ_x , whose magnitudes are listed in Table I. It is interesting to notice that \bar{x} is roughly proportional to t , whereas σ remains almost constant (the σ 's for the thinnest and thickest films are very uncertain). Furthermore, the σ 's of Table I fall inside the range $1.22 < \sigma < 1.34$, which was found previously^{1, 63, 64} to be appropriate for discontinuous noble metal films on amorphous backings. Figure 7 hence proves that a , b , and $(ab)^{1/2}$ all can be well accounted for by LNDF's which signifies⁶⁵ that—at least to a first approximation—the major and minor axes of the elliptical islands can be regarded as statistically independent entities. From the reproductive properties⁶⁶ of the LNDF we then obtain

$$\bar{x} = (\bar{a}\bar{b})^{1/2}, \quad (4)$$

which is in good correspondence with the experimental results in Table I.

An internal check on the consistency of our results for median island diameters, number of islands per unit area and area fraction can be obtained because A/n defines an average area per island. It is thus expected that a relation

$$A/n \approx (\pi/4)\bar{x}^2 \quad (5)$$

should hold at least approximately. A test of this expression is provided by Fig. 8, where the straight line represents Eq. (5). All data points fall very close to this line, indicating that our evaluations of A , n , and \bar{x} are not subject to any significant systematic errors.

B. Mean eccentricities

A quantification of the average deviation from circularity for the islands in the discontinuous films will be convenient for a description of their optical properties, as will be seen later. As a

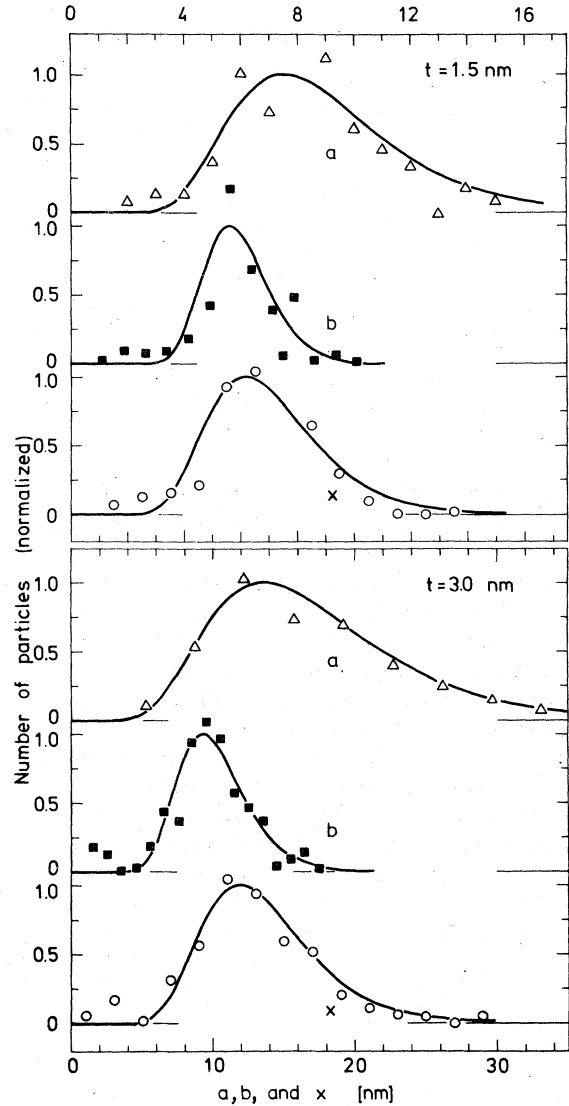


FIG. 7. Distributions of major (a) and minor (b) axes and of equivalent projected diameter ($x \equiv \sqrt{ab}$) for islands in discontinuous gold films with two average film thicknesses. The symbols denote midinterval values in size histograms based on evaluation of 300 particles at each thickness from electron micrographs of the kind shown in Fig. 2. The curves represent log-normal-distribution functions, whose median values and geometric standard deviations are contained in Table I. They are normalized so that the mode ordinates are equal to unity.

starting point the eccentricity e of an ellipse is by definition

$$e^2 = 1 - (b/a)^2. \quad (6)$$

The optical properties are not directly related to the e 's and therefore no unique mean eccentricity can be given for an ensemble of islands. However,

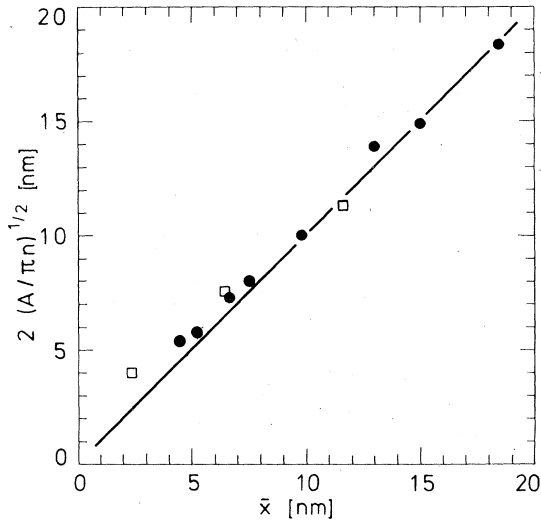


FIG. 8. Median diameter versus $2(A/\pi n)^{1/2}$ for discontinuous gold films. Filled circles signify the eight samples under present investigation. Squares denote our previous measurements reported on in Ref. 1. Straight line represents Eq. (5).

an obvious definition is to write simply

$$\bar{e}_0^2 = 1 - (\bar{b}/\bar{a})^2. \quad (7)$$

Another definition is obtained by following the reasoning in Ref. 1, where we set

$$\bar{e}^2 = 1 - \left(N^{-1} \sum_{k=1}^N \frac{a_k}{b_k} \right)^{-2}, \quad (8)$$

which puts most weight on the islands with largest elongation. Neglecting the condition $a_k \geq b_k$, which is of course a rather gross simplification, one can show that¹

$$\bar{e}^2 \approx 1 - (\bar{b}/\bar{a})^2 \exp(-4 \ln^2 \sigma). \quad (9)$$

Table I contains an evaluation of \bar{e} for those of our discontinuous films for which we were able to obtain sufficiently reliable values of \bar{a} , \bar{b} , and σ . As expected the mean eccentricity is gradually enhanced when the average film thickness is increased.

C. Three-dimensional island shapes

Up until now we have been discussing only the two-dimensional images of the islands, as seen in the electron micrographs, whereas the optical properties are governed by their three-dimensional structure. For the case of film particles represented by whole prolate spheroids (formally obtained by rotating an ellipse around its major axis) it was shown in Ref. 1 that a relation

$$t - q = \frac{2}{3} A \bar{x} (1 - \bar{e}^2)^{1/4} \exp(\frac{3}{2} \ln^2 \sigma) \quad (10)$$

should be approximately fulfilled. In Eq. (10) $t - q$ denotes an effective film thickness, which takes into account the fact that the amount of material impinging towards the substrate is not necessarily equal to the amount located on its surface as visible islands; this "lost thickness" is called q . We used the data of Table I to test the validity of Eq. (10) by plotting t versus the expression in its right member in Fig. 9. It is seen that for small t the data points lie rather accurately on a straight line (solid line), showing that a model of whole prolate spheroids is a good approximation for the three dimensional shape of the islands at $t \lesssim 3$ nm. At larger thicknesses the points fall well above the straight line, as indicated by the dashed curve. The most reasonable explanation is that the spheroidal approximation breaks down. The spheroidal model implies contact between island and substrate in one point only, which is of course unrealistic. We believe that our results should be interpreted such that the islands have a contact area much smaller than $(\pi/4)ab$, as sketched in the inset of Fig. 9.

The evaluation in Fig. 9 indicates a nonzero intercept with the abscissa for the solid line, which yields $q \approx 0.5$ nm (corresponding to less than two atomic layers of gold). This result is in keeping with the findings by Hamiltonian and Logel^{62,70,71} and by Baezold⁷² that the first few atomic layers

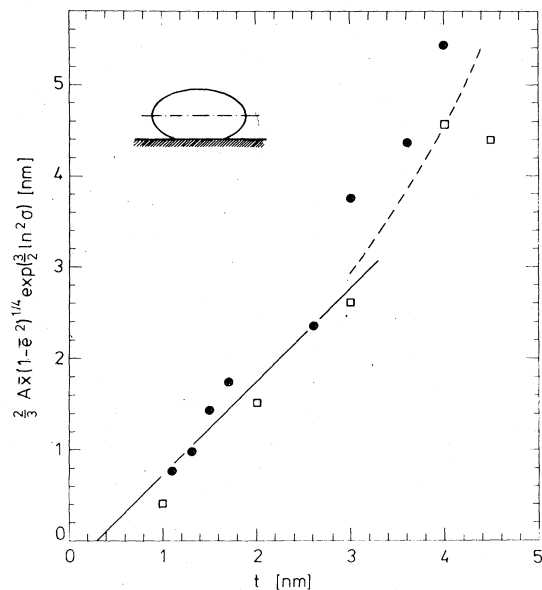


FIG. 9. Test of Eq. (10) for islands described as whole prolate spheroids. Filled circles signify the eight samples under present investigation. Squares denote our previous measurements reported on in Ref. 1. Straight line represents Eq. (10) with $q = 0.3$ nm. Inset depicts our concept of film particles on a substrate; the dash-dotted line indicates the symmetry axis.

are not contained in the discontinuous film. Possible explanations for this phenomenon include diffusion of Au into the substrate, significant re-evaporation of the deposited film, and absorbed gas layers acting as to bury the first atoms.⁷³ Still another conceivable reason for a nonzero q is that the discontinuous film forms according to the Stranski-Krastanov^{74,75} model, i.e., the first condensing atoms do not nucleate but form a layer upon which the islands then grow; this gold sheath might be lost when the substrate is dissolved in acid.

D. Average interisland distances

Not only the island sizes and shapes are important for understanding the optical properties, but also the average interisland separation is needed. One obvious experimental way of determining this quantity is to select an area containing 100 islands, say, and measuring for each of these the *smallest* center-to-center distance to its neighbours, D_{\min} . Distributions of D_{\min} are shown in Fig. 10 (open symbols and dashed curves) for films with two mass thicknesses. Another approach is to determine for each island the distances to its four nearest neighbours and associating an *average* island-to-island separation D_{ave} with the arithmetic mean of these four lengths. Distributions of D_{ave} are also given in Fig. 10 (filled symbols and solid curves). It is natural to define an unweighted average interisland distance for the entire films D by its mode.

The derivation of D , as sketched above, is rather cumbersome and an easier way of finding its magnitude would be desirable. To this end we note that the average interisland separation can be written

$$D \approx \xi(p)\bar{x}/A^{1/2} \quad (11)$$

for islands of equal diameter \bar{x} placed on a regular two-dimensional lattice such that an area fraction A is covered with islands. The prefactor $\xi(p)$ depends on the coordination number p of the lattice and it is easy to show that $\xi(6) = \pi^{1/2}/12^{1/4}$ for the hexagonal lattice, $\xi(4) = \frac{1}{2}\pi^{1/2}$ for the square lattice and $\xi(3) = \pi^{1/2}/27^{1/4}$ for the triangular lattice. Using the empirical results for \bar{x} and A we derived the corresponding D 's shown by arrows in Fig. 10. Clearly $p=4$ yields the best approximation for the average island-to-island separation. The last column in Table I gives D 's obtained from Eq. (11) with $\xi(p) \equiv \xi(4)$.

IV. EFFECTIVE-MEDIUM FORMALISM

The islands in the discontinuous films are orders of magnitude smaller than the wavelength of the incident light. Hence the optical properties of

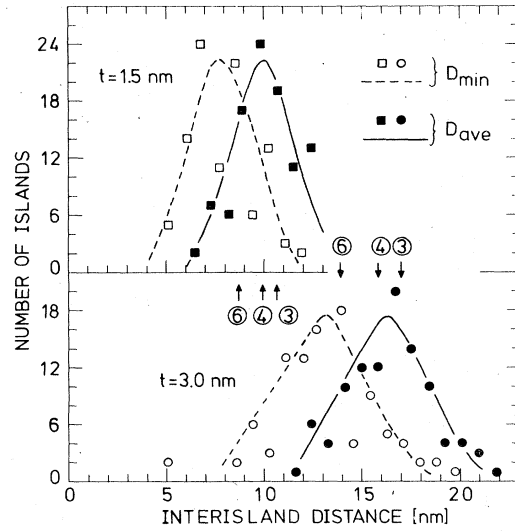


FIG. 10. Distributions of interisland separations for discontinuous gold films with two mass thicknesses. Open (filled) symbols denote histogram midpoints obtained by evaluating the minimum (average) island-to-island separation as described in the main text. The curves indicate the distributions and are drawn only as a guide to the eye. Arrows point at average interisland separations obtained from the approximate Eq. (11), with coordination number as shown by the encircled figures.

the deposits can be characterized in terms of an effective medium, being a spatial average over the dielectric permeabilities for the metal islands and for their surrounding medium. In this section we develop an effective medium approach so that it allows realistic treatments of two-dimensional arrays of ellipsoidal islands.

A Maxwell-Garnett-type theory

The Maxwell Garnett^{76,77} theory yields an effective permeability $\bar{\epsilon}$ for identical spheres according to the "standard expression"

$$(\bar{\epsilon} - \epsilon_m)/(\bar{\epsilon} + 2\epsilon_m) = f(\epsilon - \epsilon_m)/(\epsilon + 2\epsilon_m), \quad (12)$$

where ϵ is the dielectric permeability of the metal islands, ϵ_m is the dielectric permeability of their surroundings and f is the "filling factor", i.e., the volume fraction of metal in the discontinuous films (to be defined shortly). As discussed in Ref. 2 the Maxwell Garnett approach is valid when

$$(4\pi^2 x_s^2/15\lambda^2)(\epsilon + 4)(\epsilon + 2)/(2\epsilon + 3) \ll 1,$$

where x_s is the sphere diameter. This criterion holds in the case of gold for granules with sizes of the order of 10 nm or less.² The Maxwell Garnett theory also presumes that the Lorentz local-field correction applies and that the induced polarization of one particle from its neighbors is non-retarded.⁷⁸

Equation (12) implies that all islands are described by the same ϵ . However, they are sufficiently small that boundary scattering should affect significantly the mean free path of the conduction electrons, so that the dielectric function pertaining to the islands should instead be written ϵ_j , where the subscript denotes islands having a mean free path in an interval centered around l_j . A convenient way of rewriting Eq. (12) to account for this size dependence is to put²

$$\bar{\epsilon} = \epsilon_m \left(1 + \frac{2}{3} \sum_j f_j \alpha'_j \right) / \left(1 - \frac{1}{3} \sum_j f_j \alpha'_j \right), \quad (13)$$

where the f_j 's are a set of fractional filling factors, normalized by

$$\sum_j f_j = f, \quad (14)$$

and α'_j is proportional to the polarizability of the j th particles. For ellipsoids with one of their axes perpendicular to a plane but with otherwise random orientations we have

$$\alpha'_j = \frac{1}{2} \sum_{i=1}^2 \frac{\epsilon_j - \epsilon_m}{\epsilon_m + L_i(\epsilon_j - \epsilon_m)}, \quad (15)$$

where L_1 and L_2 denote the depolarization factors pertaining to the axes parallel with the plane. Equation (15), which holds only for normal incidence, was derived by Hunderi⁷⁹ in a treatment of the influence of grain boundaries and lattice defects on the optical properties of metals. Equation (15) inserted into Eq. (13) is seen to be appropriate for our morphological model of the discontinuous gold films, where we regard the islands as being prolate spheroids—characterized by a mean eccentricity \bar{e} —with their symmetry axes parallel with the substrate plane. Within this model the depolarization factors are given by⁸⁰

$$L_1 = [(1 - \bar{e}^2) / 2\bar{e}^3] \{ \ln[(1 + \bar{e}) / (1 - \bar{e})] - 2\bar{e} \}, \quad (16)$$

$$L_2 = \frac{1}{2} (1 - L_1), \quad (17)$$

or equivalent expressions in terms of \bar{e}_0 [cf. Eq. (7)].

Simpler versions of Eq. (15), referring to $L_1 = L_2 \neq \frac{1}{3}$, i.e., to islands with circular cross sections in planes parallel with the substrate, were first given by David⁸¹ in 1939 and later by Schopper^{82,83}; their approach has since become accepted almost unanimously in treatments of the optical properties of discontinuous films, as well as in some other experimental situations.^{84,85} However, the assumption $L_1 = L_2$ must be a very poor one indeed, since it is well known that electron microscopic images of the islands usually look far from round, and we find it surprising that a simplifying assumption introduced at a time when the

electron microscope was not available has survived, virtually uncriticized until now.

B. Local-field correction, filling factor, and optical thickness

The usual derivation of the Maxwell Garnett theory^{76,77} is not directly applicable to the present experimental situation because it does not incorporate the corrections to the electric field at one island from its neighbors. These local field effects, which mainly represent contributions from particles inside a Lorentz cavity, cannot be neglected on account of the small interisland distances, which imply that in particular the retarded electric dipole-dipole coupling must be significant.

One simple way of introducing a coupling among the particles is to make the effective medium theory self-consistent, which is achieved by rewriting Eq. (15) as

$$\alpha_j = \frac{1}{2} \sum_{i=1}^2 \frac{\epsilon_j - \bar{\epsilon}}{\bar{\epsilon} + L_i(\epsilon_j - \bar{\epsilon})}. \quad (18)$$

An entirely different self-consistent effective-medium theory was pioneered by Bruggeman,⁸⁶ whose approach leads to an alternative relation² for $\bar{\epsilon}$ replacing Eq. (13). A third self-consistent theory can be formulated² from the work of Hunderi.⁷⁹ The main difficulty with these three models is the fact that they are mean-field theories which represent the interactions among the particles only in so far as these can be described by a constant far field, whereas the specific near-field effects are suppressed.

The role of the distorted local field for the optical properties of island films has been discussed by Yamaguchi,⁸²⁰ Meessen,⁸⁷ and, in particular, Bedaux and Vlieger.^{43,88,89} We will follow here the approach by the latter two authors, who found that the local-field correction could be simulated by making the substitution⁴³

$$\sum_j f_j \alpha'_j \rightarrow \sum_j f_j \alpha'_j \left(1 - \frac{t}{4\langle \Lambda \rangle} \sum_j f_j \alpha'_j \right)^{-1}, \quad (19)$$

where $\langle \Lambda \rangle$ denotes an "effective" distance which is roughly equal to the separation between the centers of adjacent islands. The detailed form of the substitution (19) applies to islands in an "amorphous" configuration, and somewhat different prefactors in the denominator are encountered under other circumstances. The above substitution is equivalent to introducing "effective depolarization factors" which modify the L_i 's in Eq. (15); this kind of analysis was applied to discontinuous gold films in a couple of recent articles,^{6,33} and an intimately related approach was employed in our recent treatment² of the optical properties of ultra-

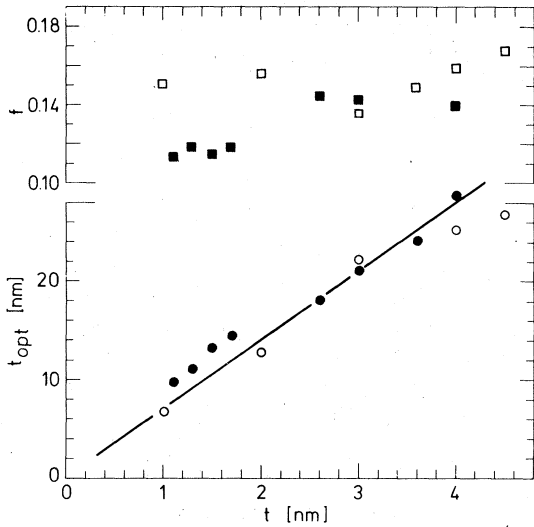


FIG. 11. "Optical" thickness (circles) and filling factor (squares) for the discontinuous gold films of the present work (filled symbols) and of Ref. 1 (open symbols). The straight line represents Eq. (22).

fine gas evaporated gold particles, where we were able to obtain excellent agreement with experimental data by taking certain fractions of the particles to be aggregated into chains and clusters.

In the present case of islands in a discontinuous film the clustering is much less significant, and we expect that one specific value of $\langle \Lambda \rangle$ suffices for a good description of the experimental facts. It is then equally correct to discuss the optical properties in terms of an "optical" thickness t_{opt} of the film as in terms of effective depolarization factors, and Bedaux and Vlieger⁴³ found that the appropriate definitions would be to put

$$t_{\text{opt}} = \frac{4}{3} \langle \Lambda \rangle \quad (20)$$

and

$$f = t/t_{\text{opt}} \quad (21)$$

in the non-self-consistent Maxwell Garnett theory.

It remains now to define $\langle \Lambda \rangle$. Bedaux and Vlieger⁴³ do not indicate any weighting of the interparticle distance in favor of the smaller or larger separations and, therefore, we feel that $\langle \Lambda \rangle \approx D$ should be the estimate which is most in line with their approach, although, upon close inspection of their calculation, it cannot be ruled out that this relation gives a somewhat too large value of $\langle \Lambda \rangle$. Figure 11 shows f and t_{opt} for our discontinuous gold films (taking $\langle \Lambda \rangle = D$) and it is found that, empirically, t_{opt} depends on mass thickness as

$$t_{\text{opt}} \approx 7.0t, \quad (22)$$

while the filling factor consistently falls at $f \approx 0.14$ with no obvious dependence on t .

C. Size-dependent dielectric permeability

The derivation of an effective dielectric permeability from Eqs. (13) and (15) implies averages over a set of size dependent dielectric permeabilities, ϵ_j . Reliable values of this quantity were obtained by starting from an accurate ellipsometric determination of the dielectric permeability for bulk gold— ϵ_{expt} , as measured by Winsemius⁹⁰—but modifying these data to account for size-dependent scattering in the free-electron (Drude) part of the dielectric function according to the construction

$$\epsilon_j = \epsilon_{\text{expt}} - \epsilon_{\text{expt}}^{\text{Drude}} + \epsilon_j^{\text{Drude}}. \quad (23)$$

The two Drude terms are given by

$$\epsilon_{\text{expt}}^{\text{Drude}} = 1 - \frac{\omega_p^2}{\omega(\omega + i/\tau_b)} \quad (24)$$

and

$$\epsilon_j^{\text{Drude}} = 1 - \frac{\omega_p^2}{\omega(\omega + i/\tau_j)}, \quad (25)$$

where ω_p is the bulk plasma frequency, τ_b is the mean electron lifetime for bulk gold, and

$$\tau_j^{-1} = \tau_b^{-1} + v_F/l_j, \quad (26)$$

where v_F is the Fermi velocity and l_j is the mean-free path for electrons in particles of size j . It should be noted that this construction leaves the interband part of ϵ_{exp} unchanged and also neglects any size quantization⁹¹⁻⁹⁶ of the conduction band. As far as we know, closed expressions for l_j exist only for spheres, where^{97,98}

$$l_j = \frac{1}{2} \kappa_{sj} \quad (27)$$

applies to diffuse boundary scattering of conduction electrons.

From Winsemius⁹⁰ the bulk properties are $\hbar\omega_p = 8.55$ eV, $\hbar/\tau_b = 0.108$ eV, $v_F/c = 4.7 \times 10^{-3}$; these values were used throughout our calculations.

D. Calculation of optical transmittance

Our calculation of optical transmittance follows the standard equations given in several books.⁹⁹ We considered a thin slab (thickness t_{opt}) comprised of islands on a Corning 7059 glass substrate, having a dielectric constant $\epsilon_s = 2.34$, as stated by the manufacturer. The transmitted intensity, T_{FS} , was computed by adding of amplitudes in the film and intensities in the substrate. Hence we excluded interference effects in the glass. We also calculated the transmitted intensity T_{SS} through an uncoated substrate. The final transmittances, which are plotted in several figures below, were derived from $T = T_{FS}/T_{SS}$.

V. CALCULATIONS AND PRELIMINARY COMPARISON WITH EXPERIMENTS

In this section we begin the detailed analysis of the optical data by comparing them with theoretical results based on the Maxwell Garnett-type effective-medium approach. The theory thus applies to islands which experience local field effects accounted for by Eq. (20) with $\langle \Lambda \rangle = D$ and are not influenced by the substrate, i.e., have $\epsilon_m = 1$.

A. Role of island shape

Figure 12 depicts calculated and measured optical transmittance for discontinuous gold films having two mass thicknesses. In the theoretical data we used four different mean eccentricities for the islands, as shown in the figure, together with f and t_{opt} as given in Fig. 11. To obtain a convenient starting point for the analysis we first calculated the transmittance for spherical islands (dash-dash-dotted curves) and compared the result with the measurements (solid curves). It is immediately clear that the two kinds of data resemble each other in so far as they both display a marked absorption band in the visible range and a high infrared transmittance. They also both reflect interband absorption as a diminished transmittance at $\lambda \approx 0.5 \mu\text{m}$. The most salient features, though, are the predicted transmittance being much too high and having a minimum falling at too short wavelength.

As we discussed earlier, an assumption of spherical islands is not supported by the electron micrographs, but a much better approximation is achieved if we postulate instead prolate spheroidal shapes governed by a mean eccentricity. Two different averagings led to the definitions of \bar{e} and \bar{e}_0 in Eqs. (7) and (8). It is obvious that $\bar{e} > \bar{e}_0$. The dotted and dashed graphs in Fig. 12 refer to using these quantities (and $l_j = \frac{1}{2}b_j$, as will be discussed shortly) in the effective-medium treatments. By going to larger mean eccentricities the transmittance minimum is seen to become deeper and shift towards larger wavelengths, but the changes are by far too small to bring the computed data into correspondence with the measurements. If we choose a very large mean eccentricity the agreement with experiments becomes improved and with a value 0.95 (dashed-dotted curves) the transmittance minimum almost coincides with the measured result, while the overall agreement is still unacceptable. It should be stressed that this latter mean eccentricity is much larger than the experimental evaluations (cf. Table I), and the most important conclusion from Fig. 12 is therefore that *the computed transmittances are much larger than the measured ones.*

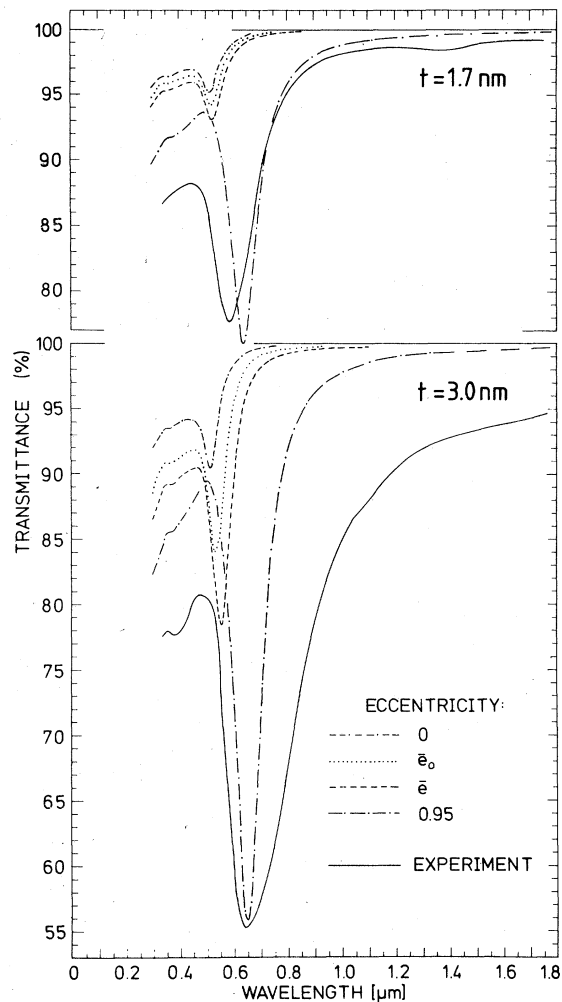


FIG. 12. Transmittance vs wavelength for discontinuous gold films with two mass thicknesses. Calculated results (variously dashed and dotted curves) refer to using f and t_{opt} as in Fig. 11, \bar{b} and σ_b as in Table I, $\epsilon_m = 1$, $\epsilon_s = 2.34$, and mean eccentricities as shown in the figure. Solid curves signify measured data (previously shown in Fig. 5).

B. Role of island size

We pointed out in Sec. IVC that the mean-free path l_j is equal to the radius in spherical islands, provided the conduction electrons experience diffuse scattering at the boundaries. No analytic expression for l_j exists for spheroids, though. It is obvious that $b_j \leq 2l_j \leq a_j$, and from the prolate shape we must expect that l_j lies closer to the lower limit than to the upper. A more exact solution, which yields l_j as a function of eccentricity, can be worked out numerically from equations given by Euler⁹⁷ (who applied them only to oblate spheroids), but it should be stressed that such a solution does not yield a "true" mean free path for the is-

lands not only because a spheroidal model is inexact but also because grain boundaries occur in particular in the larger islands. Grain boundary scattering is not incorporated via τ_b owing to the large crystallite sizes in Winsemius's bulk data.⁹⁰ The detailed influence on l_j from this effect is hard to determine, but some qualitative results can be obtained from an analysis of the electrical conduction in thin continuous metal films by Mayadas and Shatzkes¹⁰⁰ who found that grain boundaries were considerably less efficient scatterers than external surfaces. Thus l_j ought not be depressed very much from what it would be in single crystalline islands and we conclude that

$$l_j \approx \frac{1}{2} b_j \quad (28)$$

should be an accurate approximation. This substantiates the choice of l_j made in the previous computations of Fig. 12 as well as in our preliminary reports in Refs. 49 and 50. From Eq. (28) we can define a median mean free path \bar{l} , which is equal to the statistical median for the minor half axes.

With the aim of elucidating the role of mean free path on the optical transmittance we performed a series of computations by setting l_j

$= \frac{1}{4} b_j$, $l_j = \frac{1}{2} a_j$, and $l_j = a_j$ in addition to what we believe is the best estimate, namely, Eq. (28). Figure 13 shows results for a discontinuous film having a mass thickness 3.0 nm. It is evident that an enhanced mean free path produces a narrower and deeper transmittance minimum, whereas λ_{\min} is not shifted. The ultraviolet transmittance is influenced only marginally by \bar{l} , which is a manifestation of the presumed size independence of the interband contribution to ϵ_j .

The distributions of l_j employed in Fig. 13 are specified not only by their statistical medians but also by their geometric standard deviations, i.e., by σ_a or σ_b (cf. Table I) depending on which definition we take for l_j . The effect of an altered distribution width was investigated in a set of calculations where we took $\bar{l} = \frac{1}{2} \bar{b}$ but varied the geometric standard deviation from 1.0 (representing a δ -function distribution) up to 1.6, where the latter value is significantly larger than σ_b . The changes in the transmittance were too small to be shown in a diagram of the kind in Fig. 13, which is in keeping with previous results for gas evaporated gold granules (cf. Fig. 13 in Ref. 2). Clearly the islands with $l_j < \bar{l}$ give a smoothing of the transmittance dip, whereas those with $l_j > \bar{l}$ yield a

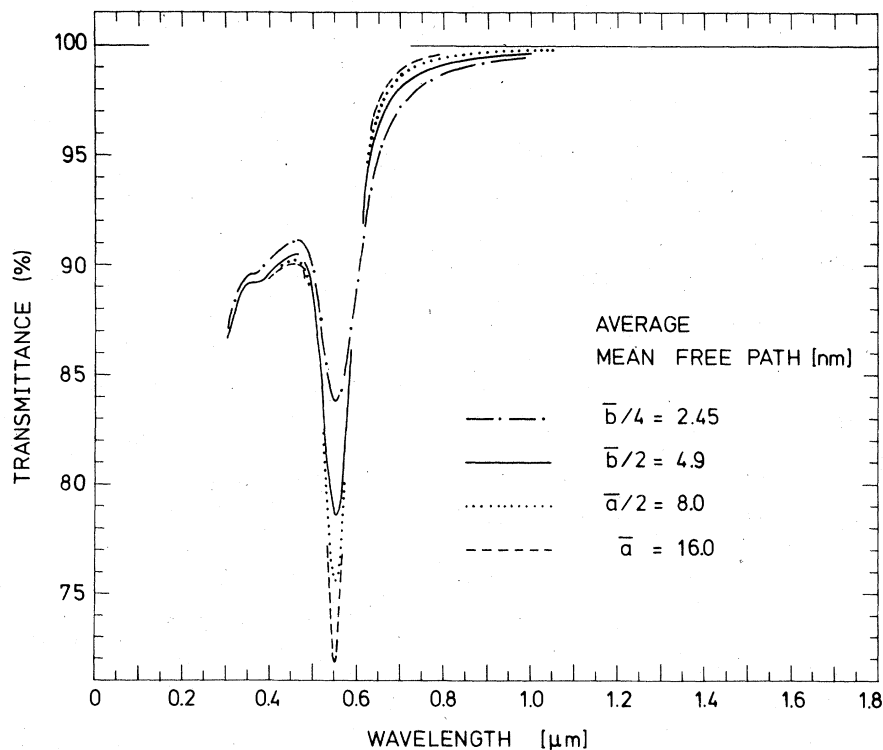


FIG. 13. Computed transmittance vs wavelength for discontinuous gold films with four different prescriptions for the average mean free path. We used parameters appropriate to the film with $t = 3.0$ nm, viz., $f = 0.142$, $t_{\text{opt}} = 21.1$ nm, $\epsilon_m = 1$, $\epsilon_s = 2.34$, and \bar{a} , \bar{b} , σ_a , σ_b , and \bar{l} as given in Table I. Solid curve is identical with the lower dashed curve in Fig. 12.

sharpening. The asymmetry of the log-normal distribution function is responsible for the cancellation of these two counteracting effects being so remarkably efficient.

C. Extension of the effective-medium formalism: Improved averaging over an ensemble of islands

Previously in this section we considered the optical absorption of islands whose deviations from spherical form were characterized by a mean eccentricity, \bar{e} or \bar{e}_0 . This approach needs justification both because the definition of a mean eccentricity is not unique and because the eccentricities of the individual islands depend to some extent on their sizes so that the largest islands tend to be most elongated (cf. also Fig. 4 in Ref. 1). To investigate the possible influence from these complicating experimental facts we must extend the effective medium formalism so that it encompasses averages over ensembles of islands described by a set of N individual (relative) volumes V_k , and eccentricities, $e_k = [1 - (b_k/a_k)^2]^{1/2}$. The appropriate generalization of Eq. (13) is then

$$\bar{\epsilon} = \epsilon_m \left(1 + \frac{2}{3} \sum_{k=1}^N V_k \alpha'_k \right) / \left(1 - \frac{1}{3} \sum_{k=1}^N V_k \alpha'_k \right), \quad (29)$$

with

$$\alpha'_k = \frac{1}{2} \sum_{i=1}^2 \frac{\epsilon_k - \epsilon_m}{\epsilon_k + L_{ik}(\epsilon_k - \epsilon_m)} \quad (30)$$

and

$$\sum_{k=1}^N V_k = f, \quad (31)$$

where the depolarization factors L_{1k} and L_{2k} are given by Eqs. (16) and (17) with k replacing j . The dielectric permeability for the k th island ϵ_k is governed by the mean free path $l_k = \frac{1}{2} b_k$.

The solid curves in Fig. 14 were calculated from the above equations by summing over islands in three randomly selected areas containing 50 islands at each mass thickness. The rather small samplings allow observations of variations of the optical properties among different regions of the discontinuous films. These data are compared with computations based on a mean eccentricity \bar{e} (dashed curves). At the smallest thickness the four curves are practically overlapping and hence a constant \bar{e} gives a very good representation for the island morphology. Furthermore, areas containing as few as 50 islands provide a good model for the overall optical transmittance. Comparing with the upper dotted curve in Fig. 12 it is seen that the agreement with the random samplings is somewhat better with \bar{e} than with \bar{e}_0 . At the larger

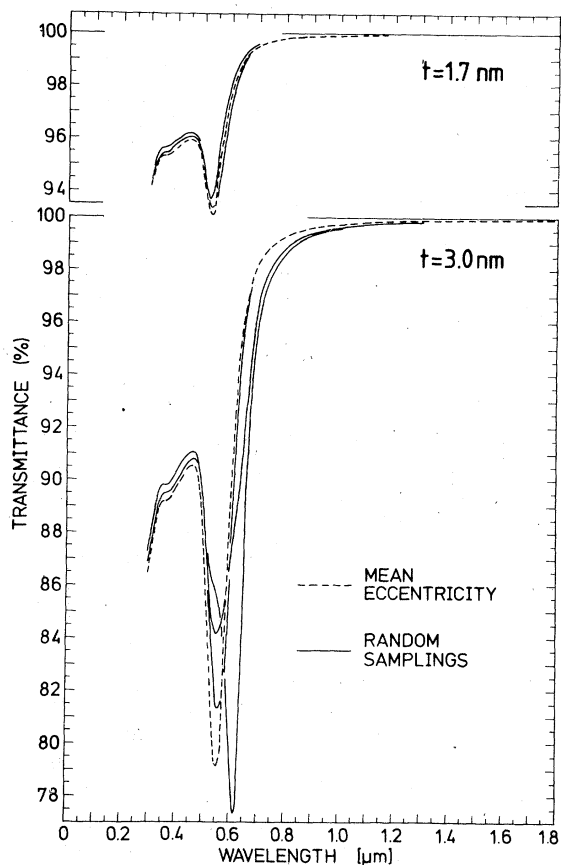


FIG. 14. Computed transmittance vs wavelength for discontinuous gold films with two mass thicknesses. Each solid curve denotes averaging over a randomly selected area containing 50 island, as described in the main text. Other parameters were f and t_{opt} as shown in Fig. 11, $\epsilon_m = 1$ and $\epsilon_s = 2.34$. Dashed curves represent calculations using constant mean eccentricities \bar{e} ; they are identical with the dashed curves in Fig. 12. Parts of the solid curves were excluded to gain clarity.

mass thickness we find from Fig. 14 that the results from different samplings over 50 islands differ noticeably, which is a manifestation of their being more irregular. Calculations with a mean eccentricity \bar{e} still gives an acceptable approximation for the optical properties.

It is important to note that the computational technique of this section does not necessarily lead to more reliable predictions than the previous simpler approach. The reason is that the largest islands in the thicker films, which dominate the absorption, are those for which the spheroidal approximation is worst. Therefore the most important conclusions of this section are the *empirical* justification of the mean eccentricity \bar{e} for the thinnest films and the qualitative result that this approach underestimates—to an unknown extent—

the width of the transmittance minimum for the thicker films.

VI. DISCUSSION

The most important result of Sec. V was the measured absorption being much larger than the computed one. The aim of this section is to clarify the origin of this enhanced absorption.

A. Effects of an interisland dielectric constant

Our effective medium formalism was written with a variable ϵ_m , which allows treatments of an interisland dielectric constant different from unity. Below we will first investigate the effects of a real $\epsilon_m > 1$ and then regard the possibility of having also an imaginary contribution.

To motivate the use of a *real* $\epsilon_m > 1$ we note that the islands must have a certain region of contact with the substrate. Hence one expects ϵ_m to fall inside an interval bounded by the dielectric constants for air and for the substrate material, i.e., $1 \leq \epsilon_m \leq \epsilon_s$. However, the common area must be small so that in reality ϵ_m ought to lie much closer to the lower limit than to the upper. Surface irregularities tend to augment the substrate interaction, but it appears doubtful whether these play any role because Corning 7059 glass is known to be extremely smooth.

The extensive literature on the optical properties of discontinuous films does not provide much to our understanding of the significance of ϵ_m , which is not surprising when one considers the insufficient sample characterizations. Actually, unanimity among different workers ends with the above interval for ϵ_m , and the disparity among various claims for the appropriate ϵ_m inside this range is exasperating. For example, Truong and Scott⁶ calculated optical properties for aggregated gold films by taking $\epsilon_m = 1$ and obtained satisfactory agreement with their experiments. In another very recent study of similar films by Jarrett and Ward³³ it was concluded from detailed comparisons of theories and experiments that $\epsilon_m = \epsilon_s$ would be appropriate. This latter choice was made also by Doremus²⁸ who found good correspondence with his experimental results. From an extensive ellipsometric investigation of discontinuous silver films by Yoshida *et al.*¹⁶ it was found that $\epsilon_m \approx \epsilon_s$ would be appropriate for $t \lesssim 2$ nm and that ϵ_m decreased for larger mass thicknesses and was practically equal to one for $t \gtrsim 8$ nm. Later the same authors revised their contention and stated¹⁸ instead that $\epsilon_m = 1$. Even more surprising is the recent claim by Tokarsky and Marton³⁸ that $\epsilon_m = 1$ would be valid for extremely thin gold films, whereas $\epsilon_m = \epsilon_s$ would be better at larger thicknesses. In addition

to the above two values for ϵ_m a definition $\epsilon_m = \frac{1}{2}(\epsilon_s + 1)$ has sometimes been adopted. This choice was introduced by David⁸¹ and has since been used in, for example, Refs. 21, 22, and 25.

Figure 15 shows our calculated results with a real interisland dielectric constant defined in three different ways, viz., $\epsilon_m = 1$, $\epsilon_m = \frac{1}{2}(\epsilon_s + 1) = 1.67$, and $\epsilon_m = \epsilon_s = 2.34$. An increased magnitude of ϵ_m is found to decrease the transmittance and shift λ_{\min} towards larger wavelengths, and when the inter-

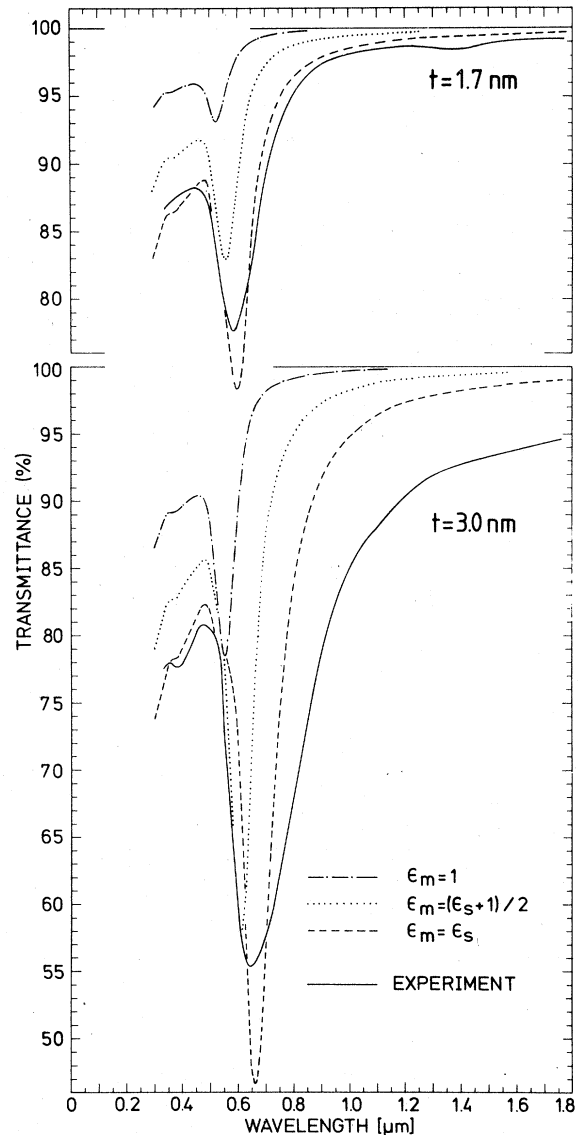


FIG. 15. Computed transmittance vs wavelength for discontinuous gold films with two mass thicknesses. We used f and t_{opt} as in Fig. 11, a real ϵ_m defined in three different ways as shown in the figure, $\epsilon_s = 2.34$ and \bar{b} , σ_b and \bar{v} as in Table I. Solid curves denote experimental data and were shown also in Fig. 5. Dash-dotted curves are identical with the dashed curves in Fig. 12.

island dielectric constant is set equal to that of the substrate we obtain a fair correspondence with the experimental data (solid curves) in particular for the thinnest film. However, this value for ϵ_m is certainly much larger than what we expect so that the good fit between theory and experiments—though striking—should nevertheless be regarded as irrelevant.

The interisland dielectric constant need not be purely real but can also have an *imaginary* part, $\epsilon_m \equiv \epsilon_{m1} + i\epsilon_{m2}$. Its most natural origin is a non-zero tunneling conductivity σ_T caused by electron transfer either through the air between adjacent islands or via the substrate.^{46,101} Expressed in terms of a finite sheet resistance, $R_\square \equiv (\sigma_T t)^{-1}$, this tunneling yields the imaginary contribution

$$\epsilon_{m2} \approx 2\lambda/R_\square ct. \quad (32)$$

As far as we know the effects of electron transfer have not been discussed previously in the context of optical properties of island films, but the mechanism has been mentioned for the related cases of optical absorption in cermet films⁸⁵ and in gas evaporated particles in metallic contact.¹⁰²

We performed computations with several values of ϵ_{m2} and with $\epsilon_{m1} = 1$. The most salient features of the transmittance curves with $\epsilon_{m2} > 0$ were the gradual decrease of the infrared transmittance and the smearing of the minimum in the visible range. For the thinnest films we found that $\epsilon_{m2} \approx 0.1$ should be an upper limit for the imaginary part; this value corresponds roughly to $R_\square \approx 2 \times 10^5 \Omega$ at optical frequencies. The dc resistance, on the other hand, was found to be $\gg 10^{12} \Omega$ from direct measurements^{45,46} on these films. The lowered infrared transmittance which we observed in the thicker films is in agreement with the results given by $\epsilon_{m2} > 0$, but if tunneling were dominating it was found from the computations that the transmittance minimum would also be smeared substantially. As a result of this analysis we conclude that electron tunneling plays a minor role at all mass thicknesses.

B. Local-field effects revisited

In this section we present a more detailed discussion of local field effects than the one in Sec. IV B, where we simply reproduced the main result from a work by Bedaux and Vlieger,⁴³ viz.,

$$t_{\text{opt}} = \frac{4}{3} \langle \Lambda \rangle = \frac{4}{3} \xi D, \quad (33)$$

with

$$\xi \equiv \xi_{\text{amorph}} \approx 1$$

for an “amorphous” distribution of islands. We first wish to elucidate the magnitude of the mul-

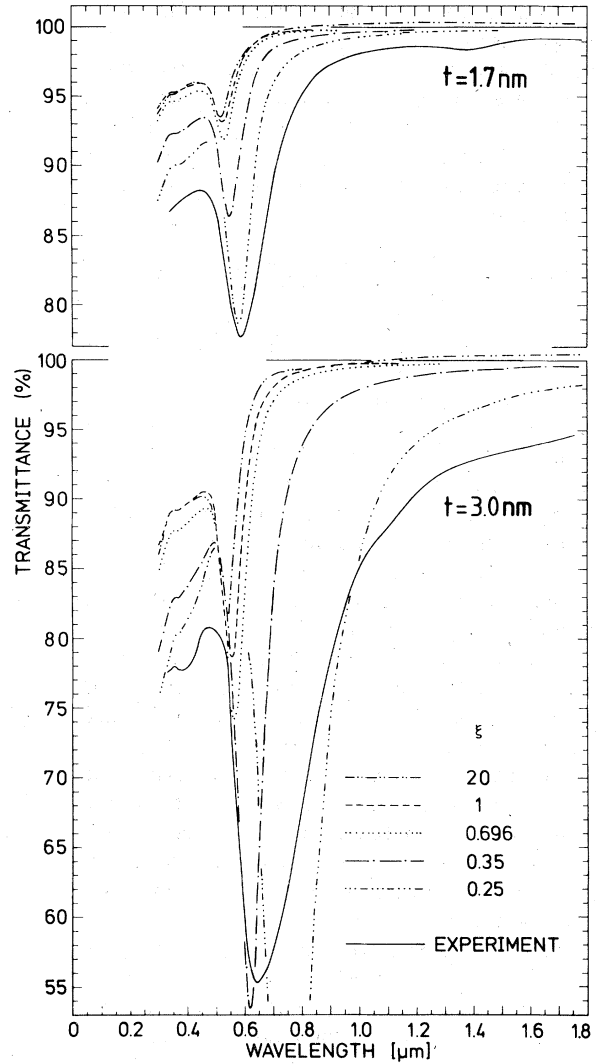


FIG. 16. Computed transmittance vs wavelength for discontinuous gold films with two mass thicknesses. We simulated changed local-field effects by having the shown values of ξ in conjunction with $\epsilon_m = 1$, $\epsilon_s = 2.34$, and \bar{b} , σ_b , and \bar{v} as in Table I. Solid curves denote experimental data and were shown also in Fig. 5. Dashed curves are identical with the dashed curves in Fig. 12.

tipple scattering effects inherent in this definition of t_{opt} , which is readily done by computing the limiting transmittance for $t_{\text{opt}} \rightarrow \infty$ and $f \rightarrow 0$ with $f t_{\text{opt}} = t$. We also employ $\epsilon_m = 1$ throughout these calculations as we do not want to introduce a further complication by substrate interaction. It is seen from the dash-dot-dotted curve in Fig. 16, applying to $\xi = 20$, that the overall transmittance is higher than when we have $\xi = 1$ (dashed curves), which is the expected result. At the largest t_{opt} 's in these calculations some weak interference effects were noted which explain the dash-

dot-dotted curves going above the 100% lines at large wavelengths.

The above value of ξ_{amorph} is rough,⁴³ and with the purpose of shedding some further light on the proper selection of an optical thickness we calculated the transmittance for islands lying on a regular square lattice where an exact solution is available. The result is^{43, 89}

$$\xi \equiv \xi_{\text{square}} = 2\pi \left(\sum_{u,v} |u^2 + v^2|^{-3/2} \right)^{-1} \approx 0.696$$

[if D in Eq. (33) denotes the lattice spacing]. Some exact results have been derived also for hexagonal lattices.¹⁰³ It is seen from the dotted curves in Fig. 16 that ξ_{square} yields a *lowered* transmittance compared with the expected result for an "amorphous" configuration of islands, which is interesting because, intuitively, one would expect the near-field effects to become smaller when the islands are kept well apart in a regular arrangement than when they can come closer to each other locally by virtue of a more random distribution. The result that $\xi_{\text{amorph}} > \xi_{\text{square}}$ does not in itself imply any inadequacy of the treatment by Bedaux and Vlieger,⁴³ though, because $\langle \Lambda \rangle$ is only roughly equal to the average interparticle separation. This indicates that it might be appropriate to use ξ as a fitting parameter, but it should then be observed that in order to achieve computed data in rough agreement with the measurements one needs $\xi \ll 1$, which is exemplified by the two curves in Fig. 16 pertaining to $\xi = 0.35$ and $\xi = 0.25$. It seems hard to justify from the results by Bedaux and Vlieger⁴³ that ξ be shifted by such a large amount and a more fundamental motivation for taking ξ as an adjustable parameter is therefore demanded, which can be obtained only by going somewhat beyond their analysis.

We note that the local field correction described by the substitution (19) contains the factor $t/\langle \Lambda \rangle$ in the denominator, which indicates that the mass thickness of the entire film would determine the local field at the islands. This is not quite correct, but *the local field is governed by the local thickness t_{loc} at the islands*, which is a function of Λ so that a more plausible substitution would be

$$\sum_j f_j \alpha_j' \rightarrow \sum_j f_j \alpha_j' / \left(1 - \frac{1}{4} \left(\frac{t_{\text{loc}}}{\Lambda} \right) \sum_j f_j \alpha_j' \right). \quad (34)$$

An appropriate definition of t_{loc} for islands with volumes $(\frac{4}{3}\pi) \bar{a} \bar{b}^2$ forming a square lattice is

$$t_{\text{loc}} = \pi \bar{a} \bar{b}^2 / 6\Lambda^2. \quad (35)$$

It is then straightforward to prove that

$$\xi = \frac{t/D}{\langle t_{\text{loc}}/\Lambda \rangle} = \frac{3t}{2A\bar{b}D^3\langle \Lambda^{-3} \rangle} \approx \frac{D^{-3}}{\langle \Lambda^{-3} \rangle} \ll 1, \quad (36)$$

where the approximate equality is well obeyed, as can be proved by inserting empirical values of A , \bar{b} , and D . The average $\langle \Lambda^{-3} \rangle$ implies a strong weighting in favor of the smallest interparticle distances, and it is therefore natural to associate the average with the mode in the distribution of *minimum* distances between the islands. Comparing the dashed and solid curves in Fig. 10 we can make a rough estimate $\xi \approx 0.5$, which proves that the magnitude of ξ is very sensitive to the detailed distributions of interparticle separations.

C Final comparison of theory and experiments

We argued that the substrate interaction would be small, although it is obvious that it cannot be totally absent because of the small parts of the islands which have to make contact with the substrate. In our final computations we used $\epsilon_m = 1.2 + i0.12$, with the imaginary part chosen to give the best overall agreement with the experiments. The fitting is not very sensitive to the detailed value of the imaginary contribution, though, and it cannot be ruled out that a purely real interisland dielectric constant would be more correct.

The enhanced local-field effects are definitely the most important cause for the increased absorption. These are accounted for by using $\xi \equiv \xi_{\text{fit}}$ as an adjustable parameter. Taking the above prescription for ϵ_m this is the *only* free parameter in our theory. Best fits between theory (circles) and experiments (solid curves) are shown in Fig. 17 where we employed the ξ_{fit} 's given in the upper part of Fig. 18. Results are given for five mass thicknesses; we excluded our two thinnest deposits since we were unable to derive reliable mean eccentricities for these as well as the thickest film which displayed very irregular islands. For the thinnest films we obtain a very satisfactory correspondence and reproduce the transmittance minimum nicely. The thicker films (with $t \geq 2.6$ nm) display too low a measured transmittance in the infrared which is indicative of a breakdown of the validity of a mean eccentricity. We stress again that it is not obvious that averaging over an ensemble of individual islands, as outlined in Sec. VC, is superior because this computational approach overestimates the influence from the largest islands. Therefore we must content ourselves with stating that the reason for the lowered infrared transmittances in the thicker deposits is their irregular islands, whose optical properties cannot be treated theoretically with any confidence.

The measured data consistently drop somewhat below the calculated results for $\lambda \approx 0.5 \mu\text{m}$, which is similar to what we observed in our previous investigation² of the optical properties of gas eva-

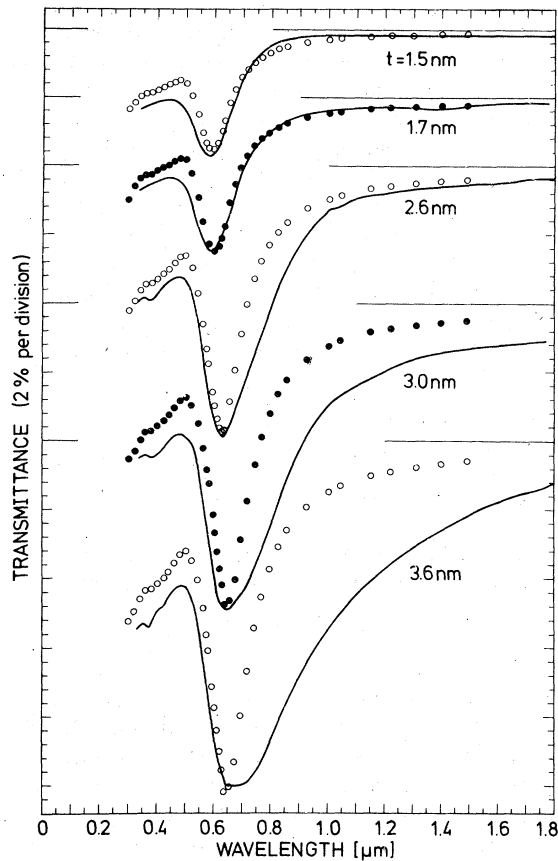


FIG. 17. Comparison of computed and measured optical transmittance (circles and solid curves) for discontinuous gold films with five mass thicknesses. The calculations refer to having the ξ_{fit} 's shown in the upper part of Fig. 18, $\epsilon_m = 1.2 + i0.12$, $\epsilon_s = 2.34$, and \bar{b} , σ_b , and $\bar{\sigma}$ as in Table I. The data points signify Winsemius's determination of the dielectric permeability for bulk gold (Ref. 90). The solid curves were shown previously in Fig. 5.

porated gold particles with diameters 3–4 nm. The most reasonable explanation—at least for the thinnest films with the smallest islands—is that this is caused by a limited-size-induced minor change of the band structure. This conclusion is supported by the absence of the tiny “shoulder” at $\lambda \approx 0.37 \mu\text{m}$ for the measured transmittances of the films with $t = 1.5 \text{ nm}$ and $t = 1.7 \text{ nm}$. Another conceivable explanation is that an absorbing gold oxide is formed on the islands. The main result of Fig. 17, however, is that *by fitting only one parameter we can achieve very satisfactory agreement with the measured transmittance*—including the absolute value and wavelength of the transmittance minimum, the width of the dip, the high infrared transmittance, and the decreased ultraviolet transmittance—and, furthermore, the existing discrepancies for the infrared transmittance of

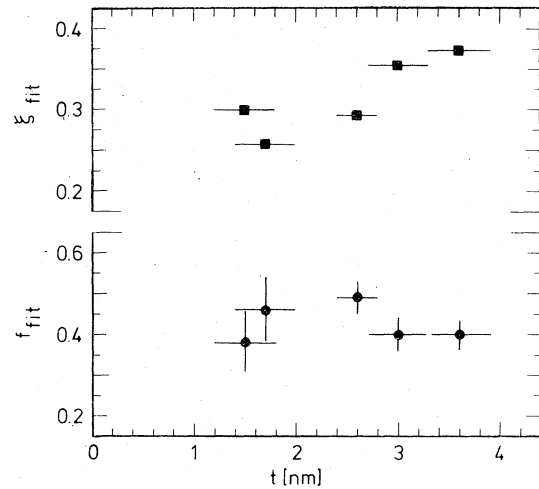


FIG. 18. Results for ξ_{fit} and f_{fit} obtained by fitting computed transmittances to measured data as shown in Fig. 17. The error bars signify the uncertainty in the determination of mass thickness.

the thicker films can be understood qualitatively though not quantitatively.

From Fig. 18 it is seen that ξ_{fit} falls inside the interval

$$0.25 < \xi_{\text{fit}} < 0.38.$$

The largest values seem to occur for the thicker deposits, although the data points are too few to allow any definite conclusions to be drawn. These empirical results are considerably lower than $\xi_{\text{square}} \approx 0.696$ referring to islands placed on a square lattice, as expected from the known sensitivity of the local-field effects to even rather narrow distributions of interparticle distances. A relation $\xi_{\text{fit}} < \xi_{\text{square}}$ is expected also because the theory by Bedaux and Vlieger⁴³ neglects dipole interaction between an island and its mirror image in the substrate.¹⁹ The fitting of computed data to experiments can be performed analogously in terms of a filling factor defined by

$$f_{\text{fit}} = 3t/4D\xi_{\text{fit}} \quad (37)$$

[cf. Eqs. (21) and (33)]. The lower part of Fig. 18 shows that this quantity lies around

$$f_{\text{fit}} \approx 0.4$$

with no strong dependence on mass thickness.

D. Oxide coatings, absorbed gases, and modified dielectric properties of the substrate

The discontinuous films have large surface-to-volume ratios which imply that even very thin *dielectric coatings* on the islands may play a noticeable role for their optical properties. The pellicles can be of two kinds: *either* the outer lay-

er on the islands can consist of a gold compound, in which case the observed spheroidal axes a_j and b_j include the oxide thickness, or the coating can be a layer of absorbed gases, which is not seen under the electron microscope so that a_j and b_j refer to the metallic cores of the islands. The effect of such coatings has been discussed by Donnadiu^{35, 104} and by Yoshida et al.^{14, 16} Below we generalize their approach so that it suits our morphological model of the discontinuous films.

We first remember that the factors α_j' in the Maxwell Garnett theory [Eq. (13)] are proportional

$$\alpha_j' = \frac{1}{2} \sum_{i=1}^2 \frac{(\epsilon_c - \epsilon_m)[\epsilon_c + (\epsilon_j - \epsilon_c)(L_i^{\text{in}} - \Omega L_i^{\text{out}})] + \Omega \epsilon_c (\epsilon_j - \epsilon_c)}{[\epsilon_c + (\epsilon_j - \epsilon_c)(L_i^{\text{in}} - \Omega L_i^{\text{out}})][\epsilon_m - L_i^{\text{out}}(\epsilon_m - \epsilon_c)] + \Omega L_i^{\text{out}} \epsilon_c (\epsilon_j - \epsilon_c)}, \quad (38)$$

where ϵ_c is the dielectric constant of the pellicles and Ω is the ratio between the volumes of the inner and outer spheroids, whose depolarization factors are L_i^{out} and L_i^{in} . These factors are, in their turn, defined from Eqs. (16) and (17) in terms mean eccentricities \bar{e}_{in} and \bar{e}_{out} , which are related by

$$(\bar{e}_{\text{out}}/\bar{e}_{\text{in}})^3 (1 - \bar{e}_{\text{in}}^2)/(1 - \bar{e}_{\text{out}}^2) = \Omega, \quad (39)$$

as follows from the spheroidal geometry. Expectedly, Eq. (38) goes over to Eq. (15) in the limits $\Omega \rightarrow 1$ and $\Omega \rightarrow 0$.

We used the above extension of the effective-medium formalism to explore the effect of compound formation on the surfaces of the islands. Gold has generally very low reactivity, but it is quite possible that a monolayer of oxide forms when the discontinuous films are kept in air; indeed, gold oxides with the compositions Au_2O , AuO , and Au_2O_3 have been mentioned in the literature.¹⁰⁶ Nothing seems to be known about their optical or electrical properties, though. In our computations we made the rather arbitrary choice $\epsilon_c \equiv \epsilon_{\text{oxide}} = 7$, which is of the same magnitude as for Cu_2O ; this value was used earlier in Ref. 2. The neglect of a possible imaginary part of ϵ_c is not very serious as it does not shift λ_{min} . For oxidized particles it is appropriate to use $\bar{e}_{\text{out}} = \bar{e}$, and \bar{e}_{in} according to Eq. (39), while the mean free paths for the conduction electrons should be determined by the minor half axes of the inner spheroids, i.e., by $\frac{1}{2}(\Omega \bar{e}_{\text{in}}/\bar{e})^{1/2} b_j$. The filling factor is not affected by the oxidation. Calculations of optical transmittance were carried out with several different values of the metal fraction Ω . The transmittance minimum was seen to shift towards larger wavelengths when Ω was decreased, whereas the overall transmittance went up. The latter result is expected because the decrease of Ω means a decrease of the volumes of the absorbing metal cores at the expense of an increase of nonabsorbing

to the polarizability of the j th islands, which indicates that in order to investigate the influence of dielectric pellicles we only have to replace Eq. (15) by its counterpart for coated spheroids, whereas all other equations can be retained. The solution of this problem demands calculating the polarizability of an ellipsoid covered with a dielectric layer of uniform thickness, which is a difficult task. However, we are interested primarily in relatively thin coatings so that confocal ellipsoids are appropriate. As shown by Bilboul¹⁰⁵ and by Donnadiu³⁵ the modified Eq. (15) then reads

oxide.

We also calculated the transmittance for islands covered with a layer of absorbed gases described by

$$\epsilon_c \equiv \epsilon_{\text{absorbed gas}} = 2.2,$$

which represents a typical dielectric constant for this situation. The coverage was simulated by having $\bar{e}_{\text{in}} = \bar{e}$, mean free path described by Eq. (28), and filling factor f/Ω , thus conserving the sizes and shapes of the metal cores and simply adding a certain amount of absorbed gases around them. Detailed computations showed that the coating produced only a very slight downwards shift of the transmittance whereas λ_{min} was practically constant.

Summarizing, we have found that dielectric pellicles can produce sizable effects only for thick oxide coverages, which were not found experimentally. Even in this case it is impossible to obtain a large shift of λ_{min} combined with the decreased transmittance demanded to fit the computed data to the experiments. Our contention is therefore that dielectric coatings play a very subordinate role for the optical properties of our discontinuous gold films.

We finally wished to check on the possible effects of *changed dielectric properties of the substrate*. These could originate from the "lost" gold atoms discussed in Sec. III C, which presumably have diffused into the substrate. This effect was explored in computations where we used several values of ϵ_s . An increased ϵ_s was found to produce a larger transmittance, but the overall changes were not very large. We expect the diffused gold atoms to be able to influence ϵ_s only marginally and our calculations hence prove that such minor modifications should play no role whatsoever for the optical properties of the discontinuous films.

VII. SUMMARY AND CONCLUDING REMARKS

The optical properties of discontinuous metal films have been treated in hundreds of papers during more than one century, and our probably incomplete listing of articles referring only to noble metal deposits contained about 40 titles published during the last two decades. This widespread interest is hardly surprising when one considers both the striking "anomalous absorption" seen in many aggregated films and the comparative ease with which the discontinuous films can be prepared and their optical properties can be tested. The basic theoretical framework for discussing these optical properties has a respectable history and goes back to work by Rayleigh¹⁰⁷ and by Maxwell Garnett.⁷⁶ A number of quantitative differences with what one expects from the simplest theories has been known for a long time, though, and the origin of these is the main reason for the continued scientific interest in the optical properties of discontinuous metal films. A detailed explanation of these discrepancies is fairly demanding and involves two steps: (i) careful characterization of the island structure, and (ii) formulation and exploitation of an accurate theoretical model for this same structure. At the outset of our work very little was known about the appropriate description of the island films, which motivated our elaborate analysis in terms of size distributions, mean eccentricities and average interparticle separations. Surprisingly, the state of the art for the theories was in better shape and we benefitted from the extensive work by, in particular, Yamaguchi, Yoshida, and Kinbara¹²⁻²⁰ and by Bedaux and Vlieger.^{43, 88, 89} They indicate how one calculates the effects of retarded dipole-dipole coupling, substrate interaction, dielectric pellicles, etc., but, owing to the general lack of proper sample characterization, we found that virtually nothing was known about the relative importance of these various mechanisms. Below we comment in some more detail on our approach to characterize the discontinuous films and compute their optical properties to the degree of accuracy manifested in the final comparison of theory and experiments in Fig. 17.

Selection of the proper metal is essential because reactive materials with thick dielectric pellicles are considerably more difficult to handle than nonreactive. Several papers report on distinct features on the optical spectra when films of Cu,^{21, 22, 35} or Ag,^{14, 21, 22, 25, 35} are kept in air, whereas no noticeable changes were seen for Au.^{21, 22, 108} The latter result is expected because thin pellicles, which are likely to form even on gold, do not affect the transmittance strongly, as

found in Sec. VID. Consequently gold should be the best choice of a nonreactive metal which is easy to evaporate.

The *overall size* of the gold islands should be sufficiently small to allow them to be treated as dipoles. As we mentioned in Sec. IVA the condition is tantamount to having linear dimensions smaller than ~ 10 nm. This condition is well obeyed only for the thinnest of our films; neither is it generally valid for a couple of recently reported^{6, 33} investigations of aggregated gold deposits. For islands larger than ~ 10 nm the Maxwell Garnett-type formalism is not strictly correct but the full complexity of Mie^{109, 110} scattering (as modified to encompass ellipsoids^{111, 112}) should be invoked.

The three-dimensional island shapes are extremely important since they influence strongly not only the location of the transmittance minimum but also the overall magnitude of the transmittance. We found from our studies of the morphology that prolate spheroids with symmetry axes along the substrate serve as an excellent approximation at least for the deposits with mass thicknesses < 3 nm. The occurrence of these particular shapes is very fortunate because ellipsoids (and also cubes¹¹³⁻¹¹⁵) are the only shapes we know how to treat theoretically. We also demonstrated that the perpendicular axes of the spheroids obeyed log-normal distributions, which allowed us to write the mean free path of the conduction electrons in terms of two parameters with the meaning of median value and standard deviation, and that a well-defined mean eccentricity and average interisland separation were sufficient to characterize the discontinuous films. The entire morphology could hence be specified by four parameters, whose magnitudes were determined from the electron micrographs. *As far as we know no similar approach to a detailed description of the island films—which is appropriate to treating their optical properties—has been published earlier.* The work which comes closest to ours in spirit is probably the one by Yoshida *et al.*¹³ who employed depolarization factors governed by a presumed log-normal distribution of the axial ratio for oblate spheroidal islands. Spheroidal islands have been discussed also in many other papers but the corresponding depolarization factors have always been introduced in a purely *ad hoc* manner instead of as determined empirically, as in the present work. It should be stressed here that our use of whole prolate spheroids to represent the islands has been documented only for the gold islands prepared by our experimental technique, viz., ultrahigh-vacuum deposition onto Corning 7059 glass. Whether or not the same morphology

is valid under other experimental conditions cannot be judged at present but should be checked carefully in each case to which the spheroidal model is applied.

The appropriate *effective-medium theory* for various inhomogeneous media is presently subject to many theoretical investigations. As we outlined in Sec. IV B such theories can be formulated in several different manners which yield differing results unless the filling factor is very small. Optical properties of three-dimensional samples (Ag-SiO₂ and Au-SiO₂ cermet films⁸⁵) were recently discussed by Abeles and Gittleman^{116, 117} who argued that the non-self-consistent Maxwell Garnett model would be superior to the self-consistent Bruggeman⁸⁶ theory. However, our more detailed investigations¹¹⁸ of the same measurements indicated that no definite conclusions as to the relative merits of these theories could be drawn owing to experimental uncertainties. A further complication is introduced by possible retardation effects.⁷⁸ Fortunately there is no need to enter these difficult matters for the two dimensional configuration of particles in a discontinuous film but we can rely on the calculations of Bedaux and Vlieger,⁴³ showing that the comparatively simple Maxwell Garnett approach is correct, provided the filling factor and optical film thickness are defined suitably.

The *computational technique* employed by us is quite elaborate. The dielectric permeability of the gold islands was specified by modifying the free-electron contribution of empirical, ellipsometric bulk data⁹⁰ to account for size-dependent electron scattering (but leaving the interband part unchanged). We believe that this approach is more accurate than a representation of the interband contribution by a sum of Lorentzians as done, for

example, in recent work by Marton and Jordan.¹¹⁹ Together with the sample characterization this provides us with a complete scheme for calculating the dielectric properties of the effective medium, from which we derived the transmittance via a procedure which incorporates multiple reflections in the film as well as in the substrate.

The *local-field effects* were first represented by strictly following the theory of Bedaux and Vlieger⁴³ (with $\xi=1$). However, this led to transmittances being significantly larger than measured results. To account for this fact we demonstrated that the local-field effects were very sensitive to distributions of interparticle separations and that a convenient representation of the enhanced local field was obtained by invoking an adjustable parameter in the formalism of Bedaux and Vlieger. This parameter also accounts for the fact that the onset of the pair correlation function for the islands, inherent in the analysis in Ref. 43 [cf. their Eq. (6.31)], should occur at a value which is somewhat smaller than D . Reasonable values of the parameter yielded very satisfactory correspondence between theory and experiments, at least as long as the islands were not too irregular. Substrate interaction is probably not totally negligible but certainly plays a subordinate role only.

Our main conclusion is that *the optical properties of discontinuous noble metal films are governed entirely by the shapes of the islands and their separation*. The bandstructure seems to be affected only marginally by the small size of the islands. No noticeable effects are caused by quantization of electronic levels. These results are supplementary to those in a previous² investigation of gas-evaporated gold particles.

¹T. Andersson and C. G. Granqvist, *J. Appl. Phys.* **48**, 1673 (1977).

²C. G. Granqvist and O. Hunderi, *Phys. Rev. B* **16**, 3513 (1977).

³M. Faraday, *Philos. Trans. R. Soc. Lond.* **147**, 145 (1857).

⁴R. S. Sennett and G. D. Scott, *J. Opt. Soc. Am.* **40**, 203 (1950).

⁵T. Sato and G. D. Scott, *J. Opt. Soc. Am.* **64**, 100 (1974).

⁶V. V. Truong and G. D. Scott, *J. Opt. Soc. Am.* **66**, 124 (1976); **67**, 502 (1977); **68**, 189 (1978).

⁷O. L. Clegg, *Proc. Phys. Soc. Lond. B* **64**, 744 (1952).

⁸S. Yamaguchi, *J. Phys. Soc. Jpn.* **15**, 1577 (1960).

⁹S. Yamaguchi, *J. Phys. Soc. Jpn.* **17**, 184 (1962).

¹⁰S. Yamaguchi, *J. Phys. Soc. Jpn.* **17**, 1172 (1962).

¹¹S. Yamaguchi, *J. Phys. Soc. Jpn.* **18**, 266 (1962).

¹²T. Yamaguchi, S. Yoshida, and A. Kinbara, *Jpn. J. Appl. Phys.* **8**, 559 (1969).

¹³S. Yoshida, T. Yamaguchi, and A. Kinbara, *J. Opt. Soc. Am.* **61**, 62 (1971).

¹⁴S. Yoshida, T. Yamaguchi, and A. Kinbara, *J. Opt. Soc. Am.* **61**, 463 (1971).

¹⁵T. Yamaguchi, S. Yoshida, and A. Kinbara, *J. Opt. Soc. Am.* **62**, 634 (1972).

¹⁶S. Yoshida, T. Yamaguchi, and A. Kinbara, *J. Opt. Soc. Am.* **62**, 1415 (1972).

¹⁷T. Yamaguchi, S. Yoshida, and A. Kinbara, *Thin Solid Films* **13**, 261 (1971).

¹⁸T. Yamaguchi, S. Yoshida, and A. Kinbara, *Thin Solid Films* **18**, 63 (1973).

¹⁹T. Yamaguchi, S. Yoshida, and A. Kinbara, *Thin Solid Films* **21**, 173 (1974).

²⁰T. Yamaguchi, S. Yoshida, and A. Kinbara, *J. Opt. Soc. Am.* **64**, 1563 (1974).

²¹G. Rasigni, *Rev. Opt.* **41**, 383, 566, 625 (1962).

²²G. Rasigni and P. Rouard, *J. Opt. Soc. Am.* **53**, 604 (1963).

- ²³P. Rouard and P. Bousquet, in *Progress in Optics*, edited by E. Wolf (North-Holland, Amsterdam, 1965), Vol. IV, p. 145.
- ²⁴P. Rouard and G. Rasigni, *Opt. Acta* **14**, 27 (1967).
- ²⁵N. Emeric and A. Emeric, *Thin Solid Films* **1**, 13 (1967-1968).
- ²⁶A. Carlan, *Ann. Phys. (Paris)* **4**, 5 (1969).
- ²⁷J. P. Gasparini and R. Fraisse, *Thin Solid Films* **30**, 111 (1975).
- ²⁸R. H. Doremus, *J. Appl. Phys.* **37**, 2775 (1966).
- ²⁹R. H. Doremus, *Thin Solid Films* **1**, 379 (1967/68).
- ³⁰R. H. Doremus, *J. Colloid Interface Sci.* **27**, 412 (1968).
- ³¹G. Henderson and C. Weaver, *J. Opt. Soc. Am.* **56**, 1551 (1966).
- ³²L. Ward, *Brit. J. Appl. Phys.* **2**, 123 (1969).
- ³³D. N. Jarrett and L. Ward, *J. Phys. D* **9**, 1515 (1976).
- ³⁴L. E. Murr, *Thin Solid Films* **3**, 32 (1969).
- ³⁵A. Donnadiu, *Thin Solid Films* **6**, 249 (1970).
- ³⁶J. P. Marton and J. R. Lemon, *Phys. Rev. B* **4**, 271 (1971).
- ³⁷J. P. Marton and J. R. Lemon, *J. Appl. Phys.* **44**, 3953 (1973).
- ³⁸R. W. Tokarsky and J. P. Marton, *J. Appl. Phys.* **45**, 3051 (1974).
- ³⁹R. W. Tokarsky and J. P. Marton, *J. Vac. Sci. Technol.* **12**, 643 (1975).
- ⁴⁰R. W. Tokarsky and J. P. Marton, *Appl. Phys. Lett.* **28**, 729 (1976).
- ⁴¹L. T. Chadderton, A. Johansen, S. Stenstrup, and L. Sarholt-Kristensen, *Radiat. Eff.* **17**, 281 (1973).
- ⁴²S. L. McCarthy, *J. Vac. Sci. Technol.* **13**, 135 (1976).
- ⁴³D. Bedaux and J. Vlieger, *Physica (Utr.)* **73**, 287 (1974).
- ⁴⁴T. Andersson, *Thin Solid Films* **29**, L21 (1975).
- ⁴⁵T. Andersson, *J. Phys. D* **9**, 973 (1976).
- ⁴⁶T. Andersson, *J. Appl. Phys.* **47**, 1752 (1976).
- ⁴⁷T. Andersson and S. Norrman, *Vacuum* **27**, 329 (1977).
- ⁴⁸T. Andersson, dissertation (Chalmers University of Technology, 1976) (unpublished).
- ⁴⁹S. Norrman, T. Andersson, C. G. Granqvist, and O. Hunderi, *Solid State Commun.* **23**, 261 (1977).
- ⁵⁰S. Norrman, T. Andersson, C. G. Granqvist, and O. Hunderi, in *Proceedings of the Seventh International Vacuum Congress and Third International Conference on Solid Surfaces*, Vienna, 1977, edited by R. Dobrozensky *et al.*, Vol. 3, p. 2075.
- ⁵¹K. L. Chopra, *Appl. Phys. Lett.* **7**, 140 (1965); *J. Appl. Phys.* **37**, 2249 (1966).
- ⁵²D. J. Kennedy, R. E. Hayes, and R. W. Alsford, *J. Appl. Phys.* **38**, 1986 (1967).
- ⁵³M. Takagi, S. Suzuki, and K. Tanaka, *J. Phys. Soc. Jpn.* **23**, 134 (1967).
- ⁵⁴K. Mihama and M. Tanaka, *J. Cryst. Growth* **2**, 51 (1968).
- ⁵⁵K. Mihama, *J. Vac. Sci. Technol.* **6**, 480 (1969).
- ⁵⁶E. Ahilea and A. A. Hirsch, *J. Vac. Sci. Technol.* **6**, 698 (1969).
- ⁵⁷E. Ahilea and A. A. Hirsch, *J. Appl. Phys.* **42**, 5601 (1971).
- ⁵⁸Y. Murayama, K. Kashiwagi, and M. Matsumoto, *J. Phys. Soc. Jpn.* **31**, 303 (1971). Conflicting results were found by L. E. Murr and H. P. Singh, *Appl. Phys. Lett.* **20**, 512 (1972).
- ⁵⁹J. C. Zanghi, M. Gauch, J. J. Métois, and A. Masson, *Thin Solid Films* **33**, 193 (1976).
- ⁶⁰L. L. Kazmerski and D. M. Racine, *J. Appl. Phys.* **46**, 791 (1975).
- ⁶¹R. M. Hill, *Thin Solid Films* **1**, 241 (1967).
- ⁶²J. F. Hamilton and P. C. Logel, *Thin Solid Films* **23**, 89 (1974).
- ⁶³C. G. Granqvist and R. A. Buhrman, *Appl. Phys. Lett.* **27**, 693 (1975).
- ⁶⁴C. G. Granqvist and R. A. Buhrman, *J. Appl. Phys.* **47**, 2200 (1976).
- ⁶⁵J. Aitchison and J. A. C. Brown, *The Lognormal Distribution* (Cambridge U.P., Cambridge, England, 1957).
- ⁶⁶R. A. Buhrman and C. G. Granqvist, *J. Appl. Phys.* **47**, 2220 (1976).
- ⁶⁷C. G. Granqvist and R. A. Buhrman, *J. Catal.* **42**, 477 (1976); **46**, 238 (1977).
- ⁶⁸J. Plestil and J. Baldrian, *Czech. J. Phys. B* **26**, 514 (1976).
- ⁶⁹J. E. Smith and M. L. Jordan, *J. Colloid Sci.* **19**, 549 (1964).
- ⁷⁰J. F. Hamilton and P. C. Logel, *Thin Solid Films* **16**, 49 (1973).
- ⁷¹J. F. Hamilton, P. C. Logel, and R. C. Baetzold, *Thin Solid Films* **32**, 233 (1976).
- ⁷²R. C. Baetzold, *J. Appl. Phys.* **47**, 3799 (1976).
- ⁷³J. A. Venables, *Thin Solid Films* **18**, S11 (1973).
- ⁷⁴E. Bauer, *Z. Kristallogr.* **110**, 372 (1958).
- ⁷⁵J. A. Venables, *Thin Solid Films* **32**, 135 (1976).
- ⁷⁶J. C. Maxwell Garnett, *Philos. Trans. R. Soc. Lond.* **203**, 385 (1904); **205**, 237 (1906).
- ⁷⁷L. Genzel and T. P. Martin, *Surf. Sci.* **34**, 33 (1973).
- ⁷⁸C. G. Granqvist and O. Hunderi, *Phys. Rev. B* **16**, 1353 (1977).
- ⁷⁹O. Hunderi, *Phys. Rev. B* **7**, 3419 (1973).
- ⁸⁰L. D. Landau and E. M. Lifshitz, *Electrodynamics of Continuous Media* (Pergamon, New York, 1969), Sec. 4.
- ⁸¹E. David, *Z. Phys.* **114**, 389 (1939).
- ⁸²H. Schopper, *Z. Phys.* **130**, 565 (1951).
- ⁸³H. Schopper, *Fortschr. Phys.* **2**, 275 (1954).
- ⁸⁴F. L. Galeener, *Phys. Rev. Lett.* **27**, 421 (1971).
- ⁸⁵R. W. Cohen, G. D. Cody, M. D. Coutts, and B. Abeles, *Phys. Rev. B* **8**, 3689 (1973).
- ⁸⁶D. A. G. Bruggeman, *Ann. Phys. (Leipzig)* **24**, 636 (1935).
- ⁸⁷A. Meessen, *J. Phys. (Paris)* **33**, 371 (1972).
- ⁸⁸J. Vlieger, *Physica (Utr.)* **64**, 63 (1973).
- ⁸⁹D. Bedaux and J. Vlieger, *Physica (Utr.)* **67**, 55 (1973).
- ⁹⁰P. Winsemius, Ph.D. thesis (Rijksuniversiteit te Leiden, The Netherlands, 1973) (unpublished).
- ⁹¹H. Fröhlich, *Physica (Utr.)* **4**, 406 (1937).
- ⁹²R. Kubo, *J. Phys. Soc. Jpn.* **17**, 975 (1962).
- ⁹³A. Kawabata and R. Kubo, *J. Phys. Soc. Jpn.* **21**, 1765 (1966).
- ⁹⁴L. P. Gor'kov and G. M. Éliashberg, *Zh. Eksp. Teor. Fiz.* **48**, 1407 (1965) [*Sov. Phys.-JETP* **21**, 940 (1965)].
- ⁹⁵L. Genzel, T. P. Martin, and U. Kreibitz, *Z. Phys.* **B 21**, 339 (1975).
- ⁹⁶M. Cini, *Surf. Sci.* **62**, 148 (1977).
- ⁹⁷J. Euler, *Z. Phys.* **137**, 318 (1954).
- ⁹⁸W. T. Doyle, *Phys. Rev.* **111**, 1067 (1958).
- ⁹⁹See, for example, O. S. Heavens, *Optical Properties of Thin Solid Films* (Dover, New York, 1965).
- ¹⁰⁰A. F. Mayadas and M. Shatzkes, *Phys. Rev. B* **1**, 1382

- (1970).
- ¹⁰¹T. J. Coutts, *Electrical Conduction in Thin Metal Films* (Elsevier, Lausanne, 1974); J. E. Morris and T. J. Coutts, *Thin Solid Films* 47, 3 (1977).
- ¹⁰²G. Zaeschmar and A. Nedoluha, *J. Opt. Soc. Am.* 62, 348 (1972).
- ¹⁰³E. C. Chan and J. P. Marton, *J. Appl. Phys.* 45, 5004 (1974).
- ¹⁰⁴J. Richard and A. Donnadieu, *J. Opt. Soc. Am.* 59, 662 (1969).
- ¹⁰⁵R. R. Bilboul, *Brit. J. Appl. Phys.* 2, 921 (1969).
- ¹⁰⁶G. V. Samsonov, *The Oxide Handbook* (IFI-Plenum, New York, 1973).
- ¹⁰⁷J. W. Rayleigh, *Philos. Mag.* 34, 481 (1892).
- ¹⁰⁸R. Philip, *C. R. Acad. Sci. Paris* 249, 1343 (1959).
- ¹⁰⁹G. Mie, *Ann. Phys. (Leipz.)* 25, 377 (1908).
- ¹¹⁰H. C. van de Hulst, *Light Scattering by Small Particles* (Wiley, New York, 1957), Chap. 9.
- ¹¹¹R. Gans, *Ann. Phys. (Leipz.)* 37, 881 (1912).
- ¹¹²S. Asano and G. Yamamoto, *Appl. Opt.* 14, 29 (1975).
- ¹¹³A. P. van Gelder, J. Holvast, J. H. M. Stoelinga, and P. Wyder, *J. Phys. C* 5, 2757 (1972).
- ¹¹⁴R. Fuchs, *Phys. Rev. B* 11, 1732 (1975).
- ¹¹⁵D. Langbein, *J. Phys. A* 9, 627 (1976).
- ¹¹⁶B. Abeles and J. I. Gittleman, *Appl. Opt.* 15, 2328 (1976).
- ¹¹⁷J. I. Gittleman and B. Abeles, *Phys. Rev. B* 15, 3273 (1977).
- ¹¹⁸C. G. Granqvist and O. Hunderi, *Phys. Rev. B* (to be published).
- ¹¹⁹J. P. Marton and B. D. Jordan, *Phys. Rev. B* 15, 1719 (1977).

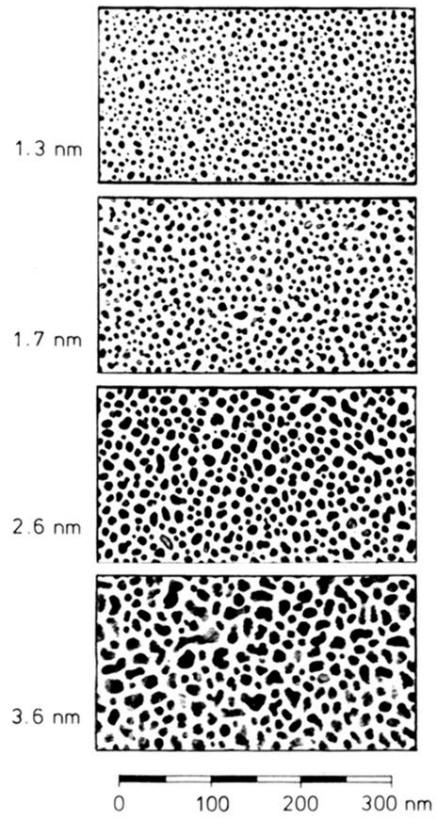


FIG. 2. High-resolution electron micrographs of discontinuous gold films at four different values of the mean film thicknesses. The figures represent regions in the middle of the deposits.